Cambridge Books Online

http://ebooks.cambridge.org/

The High-Latitude Ionosphere and its Effects on Radio Propagation

R. D. Hunsucker, J. K. Hargreaves

Book DOI: http://dx.doi.org/10.1017/CBO9780511535758

Online ISBN: 9780511535758

Hardback ISBN: 9780521330831

Paperback ISBN: 9780521041362

Chapter

Chapter 3 - Fundamentals of terrestrial radio propagation pp. 113-180

Chapter DOI: http://dx.doi.org/10.1017/CBO9780511535758.005

Cambridge University Press

Chapter 3

Fundamentals of terrestrial radio propagation

3.1 Introduction

Since we are concerned with the propagation of radio waves over the entire radio spectrum at high latitudes, it should be useful to review the basic physics and terminology of the propagation of radio waves in general. The radio spectrum extends from the extra-low-frequencies (ELF) band through microwaves and millimeter waves. Table 3.1 shows the radio spectrum from ~30 Hz to 30 GHz, along with the International Telecommunications Union (ITU) band designations.

3.2 Electromagnetic radiation

3.2.1 Basics of line-of-sight propagation *in vacuo*

An example of line-of-sight (LOS) propagation is that between two spacecraft in deep space where the medium is virtually a vacuum. The refractive index is unity and the speed of an electromagnetic (EM) wave is independent of its frequency and equal to the speed of light.

By definition, an isotropic radiator is one that radiates equally in all directions. If power P is radiated, the power density S (the power crossing unit area) at a distance d from the source is

$$S = P/(4\pi d^2), \tag{3.1}$$

Downloaded from Cambridge Books Online by IP 141.211.4.224 on Wed Mar 23 15:38:40 GMT 2016.
http://dx.doi.org/10.1017/CBO9780511535758.005
Cambridge Books Online © Cambridge University Press, 2016

From EM theory, the vector **S** is the Poynting flux, given by

$$\mathbf{S} = \mathbf{E} \times \mathbf{H}, \tag{3.2}$$

Table 3.1. *The radio spectrum (as defined by the International Telecommunications Union (ITU)), primary modes of propagation, and effects of the terrestrial ionosphere*

ITU designation	Frequency range	Principal modes of propagation	Principal uses
Extra-low-frequency (ELF)	30–300 Hz	Groundwave and Earth–ionosphere waveguide mode	Submarine communication
Very-low-frequency (VLF)	3–30 kHz	Same as above	Navigation, standard frequency and time dissemination
Low-frequency (LF)	30–300 kHz	Same as above	Navigation LORAN-C[a]
Medium-frequency (MF)	300–3000 kHz	Primarily groundwave, but skywave[b] at night	AM broadcasting, maritime, aeronautical communication
High-frequency (HF)	3–30 MHz	Primarily skywave, some groundwave	Shortwave broadcasting, amateur, fixed services
Very-high-frequency (VHF)	30–300 MHz	Primarily LOS, some skywave at lower VHF	FM broadcasting, television, aeronautical communication
Ultra-high-(UHF) frequency	300–3000 MHz	Primarily LOS, some refraction and scattering by the ionosphere	Television, radar, navigation[c], aeronautical communication
Super-high-(SHF) frequency	3–30 GHz	Same as above	Radar, space communication

Notes:

[a] The LORAN-C system will probably be superseded by the GPS system.

[b] "Skywave" denotes the Earth–ionosphere–Earth-reflected mode.

[c] Global Positioning System of satellite constellation.

Downloaded from Cambridge Books Online by IP 141.211.4.224 on Wed Mar 23 15:38:40 GMT 2016.
http://dx.doi.org/10.1017/CBO9780511535758.005
Cambridge Books Online © Cambridge University Press, 2016

E being the electric vector and **H** the magnetic vector. Since

$$E/H = 120\pi \tag{3.3}$$

for an EM wave, E and H being, respectively, the electric and magnetic field strengths,

$$S = E^2/(120\pi). \tag{3.4}$$

Therefore,

$$E = \sqrt{30P}/d. \tag{3.5a}$$

In SI units, P is in watts, d in meters, S in W m^{-2}, and E in V m^{-1}. It may be more practical to express d in kilometers, P in kilowatts, and E in mV m^{-1}, in which case

$$E\,(\text{mV m}^{-1}) = 173\ \sqrt{P\,(\text{kW})}\ /d\,(\text{km}). \tag{3.5b}$$

If the antenna does not radiate isotropically, it is said to have a gain (G), given by the ratio of the Poynting flux at a point on the axis divided by the flux that would be received at the same point if the same power were radiated instead from an isotropic radiator. If an antenna with gain G_t transmits power P_t and the receiving antenna has aperture A_r (m^2), the power received is

$$P_r = A_r S = A_r G_t P_t/(4\pi d^2) \tag{3.6}$$

and

$$E_r = \sqrt{30 P_t A_r G_t}/d. \tag{3.7}$$

Antenna theory shows that gain and aperture are related by

$$G = 4\pi A/\lambda^2, \tag{3.8}$$

in which A is the true aperture if the antenna has the form of an efficient dish, but may be an *effective* area otherwise. An isotropic radiator (which is hypothetical in any case for an EM wave) has unity gain and effective area $\lambda^2/(4\pi)$. For a half-wave dipole, which may be taken as the reference, $G = 1.64$ and

$$A = 1.64\lambda^2/(4\pi) = 0.1305\lambda^2.$$

In a point-to-point link it is often convenient to represent the reduction of signal due to the separation (d) between transmitting and receiving antennas as the *free-space attenuation*,

$$L_b = 20\log(4\pi d/\lambda), \tag{3.9}$$

which follows from Equations (3.6) and (3.8) assuming that both antennas are isotropic radiators. The gain (sometimes called directivity) is given approximately by

$$G = 30000/(\theta\phi), \tag{3.10}$$

Downloaded from Cambridge Books Online by IP 141.211.4.224 on Wed Mar 23 15:38:40 GMT 2016.
http://dx.doi.org/10.1017/CBO9780511535758.005
Cambridge Books Online © Cambridge University Press, 2016

where θ and ϕ are the half-power beamwidths (in degrees) in the E and H planes, respectively, assuming that there are no sidelobes. The formula applies only up to 20° beamwidth.

Although it is an important topic in radio propagation, a full discussion of antennas would be outside the scope of this book. Some of the many treatments are listed in the references. Information on radiation patterns and advice on siting are contained in the publications of the American Radio Relay League (ARRL) in the references. For detailed discussions of Fresnel-zone siting fundamentals, bandwidth, and terrain effects see Appendix A7 of Hunsucker (1991), Freeman (1997), or Wolff (1988). Computer programs for antenna design and performance analysis are listed in Table 3.2 and in Balanis (1997).

3.2.2 Principles of radar

In radar a transmitted signal is reflected from a target and then detected by a receiver, which may but need not be co-located with the transmitter. These are *monostatic* and *bistatic* systems, respectively. The target may be a solid object (Figure 3.1) or a distributed scattering medium (as in coherent and incoherent

Table 3.2. *Antenna design and performance-analysis programs*

Name of software	Description	Source
NEC	Numerical electromagnetic code	
NEC/WIRES 1.5	One version of NEC	Brian Beezley 3532 Linda Vista Dr., San Marcos, CA 92069, USA
NEC/Yagis 2.0	Uses NEC to model Yagis and arrays of Yagis	″ ″
YO 6.0	Optimizes Yagi–Uda designs	″ ″
AO 6.0	Optimizes antenna designs for any wire-or tubing-type antenna	″ ″
ELNEC		
MININEC		
GAP, BIA, ACP, and Phased Array Program	General Antenna Program, Beam Intermodulation Analyzer, Antenna Coverage Program, and Phased Array Program	COMSAT antenna lab suite http://www.comsat. Com/Corp/lab/labs.html
XFDTD 4.0	User-friendly electromagnetics software, covers more esoteric antennas, scattering, etc.	REMCOM Inc. http://www.remcominc.com

Downloaded from Cambridge Books Online by IP 141.211.4.224 on Wed Mar 23 15:38:40 GMT 2016.
http://dx.doi.org/10.1017/CBO9780511535758.005
Cambridge Books Online © Cambridge University Press, 2016

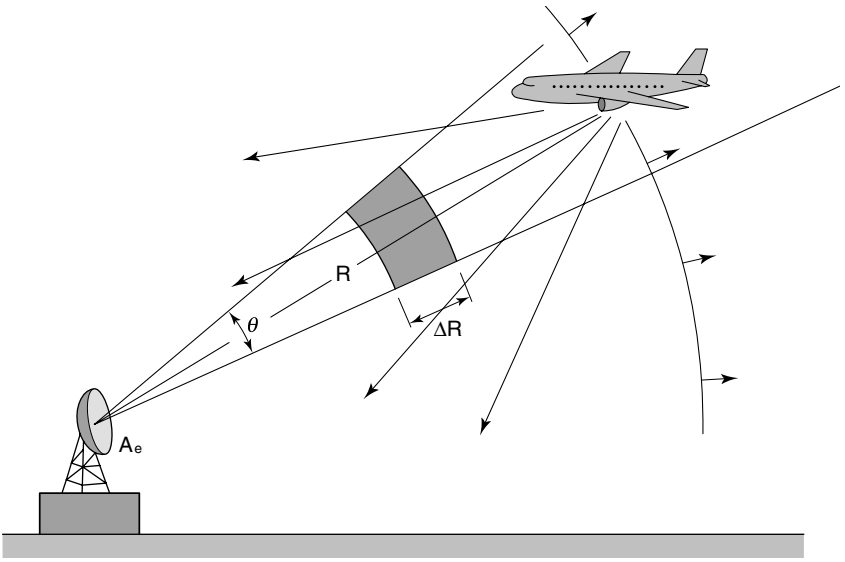

Figure 3.1. A schematic diagram of the radar principle.

scatter radars – Sections 4.2.2 and 4.2.3). A treatment of radar begins with the *radar equation.*

If power P_t is radiated by the transmitter using an antenna with gain G, the power density at a target at distance R is (Equation (3.6))

$$S = GP_t/(4\pi R^2). \tag{3.11}$$

If the target has cross-section σ, and the power intercepted is scattered equally in all directions, the power received back at the radar is

$$\begin{aligned} P_r &= GP_t/(4\pi \mathrm{R}^2) \times \sigma \times A_e/(4\pi R^2) \\ &= GP_t A_e \sigma/[(4\pi)^2 R^4] \end{aligned} \tag{3.12}$$

where A_e is the effective area of the radar antenna. (If the scattering is not omni-directional, this is taken into account in the value of σ.) From Equation(3.8) we may also write the radar equation as

$$\begin{aligned} \frac{P_r}{P_t} &= \frac{G^2\sigma}{4\pi}\frac{\lambda^2}{4\pi R^2} \\ &= G^2\lambda^2\sigma/(64\pi^2 R^4). \end{aligned} \tag{3.13}$$

The distance beyond which the target cannot be detected is the *maximum radar range,* R_{max}, and the limit is when the received echo power, P_r, just equals the *minimum detectable signal,* S_{min}. Hence (from Equation (3.12)),

Downloaded from Cambridge Books Online by IP 141.211.4.224 on Wed Mar 23 15:38:40 GMT 2016.
http://dx.doi.org/10.1017/CBO9780511535758.005
Cambridge Books Online © Cambridge University Press, 2016

$$R_{max} = \{P_t G A_e \sigma/[(4\pi)^2 S_{min}]\}^{1/4}, \tag{3.14a}$$

which is the most common form of the radar range equation.

Using Equation (3.8) gives the alternative forms

$$R_{max} = \{P_t G^2 \lambda^2 \sigma/[(4\pi)^3 S_{min}]\}^{1/4} \tag{3.14b}$$

and

$$R_{max} = [P_t A_e^2 \sigma/(4\pi\lambda^2 S_{min})]^{1/4}. \tag{3.14c}$$

The foregoing discussion applies to situations like that in Figure 3.1, where the target is smaller than the transmitter beamwidth. The larger the target, the more power is returned. If the scattering region is larger than the beamwidth (a *beam-filling target*), as may happen when the ionosphere is the target, all the incident power is intercepted and then the expression for the echo power received back at the radar has the form

$$P_r = P_t \sigma A_e/(4\pi R^2), \tag{3.15}$$

where σ represents the scattering property of the target medium. The echo power now varies as R^{-2} instead of R^{-4}. If the ionosphere is the target, the return would probably come from a large number of individual scatterers, and the σ would include the number of scatterers within the radar pulse and beamwidth at any one time, as well as their directional properties.

The physical length of the transmitted pulse (Figure 3.1) is

$$\Delta R = c\tau, \tag{3.16}$$

c being the speed of light *in vacuo* and τ the pulse duration. The resolution in range is $\Delta R/2$.

Discussions of the various forms of the radar equation and their implications, including theorems applicable to "soft targets," are given by Skolnik (1980) and by Hunsucker (1991; pp. 38–39).

3.2.3 The significance of the refractive index

A simple propagating wave

If a radio source generates an electric field $E = E_0 \cos(\omega t)$, which propagates at speed v in the z direction, the field at a distance z from the source is

Downloaded from Cambridge Books Online by IP 141.211.4.224 on Wed Mar 23 15:38:40 GMT 2016.
http://dx.doi.org/10.1017/CBO9780511535758.005
Cambridge Books Online © Cambridge University Press, 2016

$$\begin{aligned} E &= E_0 \cos[\omega(t - z/v)] \\ &= \mathrm{E}_0 \cos[\omega(t - kz)] \\ &= \mathrm{E}_0 \cos[2\pi(t/T - z/\lambda)] \end{aligned} \tag{3.17}$$

since $\omega = 2\pi f$, $v = \lambda f$, and $k = 2\pi/\lambda$ by definition. T is the period, ω and f are the frequency in radians s^{-1} and hertz, respectively, and k is the *wave number*, *propagation constant*, or *phase-shift factor.* E is the instantaneous value of the electric field at (t, z) and E_0 is the *amplitude* of the electric field. Plainly, the same phase repeats itself every $T\,(= 1/f)$ in time and every $\lambda = 2\pi/k$ in distance. For the propagation of a plane wave in three dimensions, k can be regarded as a vector along the propagation direction, having components k_x, k_y, and k_z that give the wavelengths in the x, y, and z directions and thus the phase velocities $v_x = \lambda_x f$, $v_y = \lambda_y f$, and $v_z = \lambda_z f$.

The refractive index

We will use v_p to denote the phase velocity, and for an EM wave its value depends on the nature of the medium;

$$v_\mathrm{p} = 1/(\mu\varepsilon)^{1/2}, \tag{3.18}$$

where μ and ε are the permeability and permittivity of the medium. In free space this becomes

$$c = 1/(\mu_0\, \varepsilon_0)^{1/2} = 3 \times 10^8 \text{ m s}^{-1}, \tag{3.19}$$

where μ_0 and ε_0 are, respectively, the permeability and permittivity of free space. The ratio $n = c/v$ is the *refractive index* of the medium, and the propagating wave may then be written

$$E = \mathrm{E}_0 \cos(t - nz/c). \tag{3.20}$$

If the refractive index varies with the wave frequency, the medium is said to be *dispersive.* A modulated wave is not monochromatic, and in a dispersive medium the modulation travels not at the phase velocity but at the *group velocity* (u), which is related to the phase velocity by

$$u = (\partial k/\partial\omega)^{-1}. \tag{3.21}$$

Only if v_p is independent of ω, so that $k = \omega/v_\mathrm{p}$, does $u = v_\mathrm{p}$.

Propagation in a lossy medium

If the medium absorbs energy from the wave, the amplitude decreases with distance as $\exp(-\kappa z)$, where κ is the *absorption coefficient*, and the amplitude

Downloaded from Cambridge Books Online by IP 141.211.4.224 on Wed Mar 23 15:38:40 GMT 2016.
http://dx.doi.org/10.1017/CBO9780511535758.005
Cambridge Books Online © Cambridge University Press, 2016

decreases by a factor of e over a distance $1/\kappa$. It is convenient here to use the j notation, writing

$$E = E_0 \exp[\mathrm{j}\omega(t - nz/c)], \tag{3.22}$$

where $\mathrm{j} = \sqrt{-1}$, and it is understood that the real part is taken (since $\mathrm{e}^{\mathrm{j}\theta} = \cos\theta + \mathrm{j}\sin\theta$). Taking a complex refractive index

$$n = \mu' - \mathrm{j}\chi \tag{3.23}$$

($'$ has been added to μ to avoid confusion with the permeability), gives

$$E = E_0 \exp[\mathrm{j}\omega(t - \mu' z/c)] \exp(-\chi\omega z/c). \tag{3.24}$$

Hence, the real part of the refractive index determines the velocity of the wave, and the imaginary part gives the absorption coefficient

$$\kappa = \omega\chi/c = 2\pi\chi/\lambda_0, \tag{3.25}$$

λ_0 being the free-space wavelength.

Alternatively, we may introduce a *complex propagation constant*,

$$\gamma = \mathrm{j}k = \alpha + \mathrm{j}\beta \tag{3.26}$$

giving

$$\begin{aligned} E &= E_0 \exp[\mathrm{j}(\omega t + \mathrm{j}\gamma z) \\ &= E_0 \exp[\mathrm{j}(\omega t - \beta z)] \exp(-\alpha z). \end{aligned} \tag{3.27}$$

Thus, comparing with Equations (3.24) and (3.25),

$$\beta = \omega\mu'/\mathrm{c};\ \alpha = \omega\chi/c = \kappa.$$

Conductivity

For a partial conductor the absorption is related to the conductivity, σ, and it can be shown (Hunsucker, 1991, pp. 25–31) that

$$\gamma = \omega\sqrt{\mu(\mathrm{j}\sigma/\omega - \varepsilon)}. \tag{3.28}$$

Squaring, and equating real and imaginary parts, gives

$$\alpha = \frac{\omega\sqrt{\mu\varepsilon}}{\sqrt{2}} \left[\left(1 + \frac{\sigma^2}{\omega^2\varepsilon^2} \right)^{1/2} - 1 \right]^{1/2} \tag{3.29}$$

Downloaded from Cambridge Books Online by IP 141.211.4.224 on Wed Mar 23 15:38:40 GMT 2016.
http://dx.doi.org/10.1017/CBO9780511535758.005
Cambridge Books Online © Cambridge University Press, 2016

and

$$\beta = \frac{\omega\sqrt{\mu\varepsilon}}{\sqrt{2}}\left[\left(1+\frac{\sigma^2}{\omega^2\varepsilon^2}\right)^{1/2}+1\right]^{1/2}. \tag{3.30}$$

The units of α and β are nepers m^{-1} and radians m^{-1}, respectively.

If, in (3.28), $\varepsilon \gg \sigma/\omega$, the medium approximates a pure dielectric. If $\varepsilon \ll \sigma/\omega$, the medium approximates a conductor. There is a *cross-over frequency* given by

$$\omega = \sigma/\varepsilon. \tag{3.31}$$

Evanescent waves

Going back to Equation (3.23), it is possible for the refractive index to be purely imaginary, so that $n = -j\chi$, and then

$$E = E_0 \exp(j\omega t)\exp(-\chi\omega z/c). \tag{3.32}$$

This is an *evanescent wave,* which extends into the medium by about $c/(\chi\omega)$ but does not propagate because its phase does not vary with distance. When a propagating wave is totally reflected at the interface between two media, an evanescent wave exists just inside the second medium.

3.2.4 Interactions between radio waves and matter

The basic interactions are reflection, refraction, dispersion, diffraction, scattering, change of polarization, and attenuation; and these – singly or in combination – are the processes which underlie the various phenomena of terrestrial radio propagation. They have also provided us with a number of well-proven techniques for the investigation of the propagation media and their behavior, knowledge of which is essential to the understanding of radio communication and its problems.

Reflection occurs at the boundary between two media, returning energy back towards the source in the case of normal incidence, whereas *refraction* causes any transmitted ray to emerge at an angle to the incident ray. These effects are discussed in the context of ionospheric reflection in Section 3.4.3, and of the partial reflection technique in Section 4.2.4.

Dispersion, the variation of velocity with frequency, has consequences for the transmission of information (Section 3.4.1).

Diffraction phenomena occur when there are irregularities in the propagating wavefront, causing the wavefront to evolve as the wave travels on. It is the basis of *radio scintillation* (Section 3.4.5).

Scattering from structures in the medium that are small relative to the wavelength of the incident wave diverts some fraction of the incident signal over a wide range of directions. It is the basis of communication over scatter links (Section

Downloaded from Cambridge Books Online by IP 141.211.4.224 on Wed Mar 23 15:38:40 GMT 2016.
http://dx.doi.org/10.1017/CBO9780511535758.005
Cambridge Books Online © Cambridge University Press, 2016

8.5). Also, a (usually weak) echo may be detected at the transmitter site, which is utilized in the techniques of *coherent* and *incoherent scatter* radars described in Section 3.5 and in Sections 4.2.2 and 4.2.3.

Polarization changes occur in an ionized medium in the presence of a geomagnetic field. There are consequences for the design of transmitting and receiving antennas and polarization may be exploited in ionospheric measurements (Sections 3.4.1 and 3.4.4).

Attenuation is, of course, undesirable in communications, often setting the lower limit to the usable frequency band. Measurements of absorption may give useful information, particularly about the lower ionosphere (Sections 3.4.4 and 4.2.4).

3.3 Propagation through the neutral atmosphere

3.3.1 The refractivity of the neutral atmosphere

Although this book is primarily concerned with the high latitude ionosphere and its effects upon radio propagation, there are some tropospheric effects peculiar to high latitudes that affect radio propagation in the *line-of-sight* (LOS) and earth-to-satellite modes. For that reason, we will briefly discuss some of the fundamentals of these modes. We will exclude the *troposcatter* propagation mode in which forward scatter in the troposphere (3–8 km height) permits communication over path-lengths from ~300 to 600 km, using frequencies from 200 MHz to 10 GHz (see Norton and Wiesner, 1955; and Collin, 1985). Radio waves propagating in the troposphere are affected by the refractive index, n – which is a function of atmospheric pressure, temperature, and humidity, and, near the Earth's surface at VHF/UHF, n is approximately 1.0003. It is convenient to define a *radio refractive index*, N, as

$$N = (n - 1) \times 10^6. \tag{3.33}$$

Since the terrestrial atmosphere varies exponentially with height, we may express it as

$$N(h) = N_s \exp(-ch), \tag{3.34}$$

where N_s is the surface refractivity, h is the height above the surface in kilometers, $C = \ln(N/N_s) + \Delta N$, and ΔN is the difference between the values of N at a height of 1 km above the surface and at the surface.

N_s may be estimated from

$$-\Delta N = 7.32 \exp(0.005\,577 N_s). \tag{3.35}$$

A useful parameter, the *effective Earth-radius* (the actual Earth-radius corrected for "normal" atmospheric refraction) for radio propagation is given by

Downloaded from Cambridge Books Online by IP 141.211.4.224 on Wed Mar 23 15:38:40 GMT 2016.
http://dx.doi.org/10.1017/CBO9780511535758.005
Cambridge Books Online © Cambridge University Press, 2016

Table 3.3. *CRPL exponential radio-refractivity atmospheres,* $N = N_s exp(-ch)$

N_s	$-\Delta N$	K	C
200	22.331 77	1.177 69	0.118 399
250	29.331 77	1.250 16	0.125 626
289	36.684 83	1.333 24	0.135 747
300	39.005 79	1.362 80	0.139 284
320	43.603 42	1.425 87	0.146 502
350	51.550 41	1.551 05	0.159 332
400	68.129 50	1.907 66	0.186 719
450	90.010 56	2.777 61	0.223 256

$$K = \left(1 - \frac{r_0}{n_s} c N_s \times 10^{-6}\right)^{-1} \tag{3.36}$$

where $n_s = 1 + N_s \times 10^{-6}$, r_0 is the Earth-radius = 6373.02 km, $N_s = 289$, and $c = 0.136$, so $K = 1.333\,241\,0$, or 4/3.

The basic exponential reference atmosphere is defined by the relation

$$N(h') = 289 \exp(-0.136 h'), \tag{3.37}$$

where h' is the height above the surface in kilometers.

Table 3.3 shows the CRPL (the old Central Radio Propagation Lab – now the Institute for Telecommunication Sciences (ITS) – in Boulder, Colorado) exponential radio refractivity atmosphere. The standard model of the atmosphere is obtained by assuming that N decreases linearly over the first kilometer above the surface:

$$N = N_s + \Delta N(h - h_s); \qquad h_s < h < (h_s + 1), \tag{3.38}$$

where ΔN is from Equation (3.34), h is the height above sea level, h_s is the height of the surface above mean sea level in kilometers and ΔN is the difference between N_s and N 1 km above the Earth's surface. The constants adopted for the standard atmosphere are given in Table 3.4. N can be calculated from radiosonde data:

$$N = 77.6P/T + 3.73 \times 10^5 e/T^2 = \text{“dry term”} + \text{“wet term”}, \tag{3.39}$$

where P is the atmospheric pressure in millibars, e is the vapor pressure in millibars, and T is the temperature in kelvins.

A set of “standard atmospheres” showing the height dependence of radio

Downloaded from Cambridge Books Online by IP 141.211.4.224 on Wed Mar 23 15:38:40 GMT 2016.
http://dx.doi.org/10.1017/CBO9780511535758.005
Cambridge Books Online © Cambridge University Press, 2016

Table 3.4. *Constants for the standard reference atmosphere*

N_s	h_s (ft)	a' (miles)	$-\Delta N$	K	a_e (miles)	c (km)
0	0	3960.0000	0	1.00000	3960.00	0
200	10000	3961.8939	22.3318	1.16599	4619.53	0.106211
250	5000	2960.9470	29.5124	1.23165	4878.50	0.114559
301	1000	3960.1894	39.2320	1.33327	5280.00	0.118710
313	900	3960.1324	41.9388	1.36479	5403.88	0.121796
350	0	3960.0000	51.5530	1.48905	5896.66	0.130579
400	0	3960.0000	68.1295	1.76684	6996.67	0.143848
450	0	3960.0000	90.0406	2.34506	9286.44	0.154004

Note:
a_e is the effective Earth-radius and is equal to the product aK.
$a' = a + h_s$, where h_s is the height of the Earth's surface above sea level.
$a = 3960$ miles.

$$c = \frac{1}{8 - h_s} \ln\left(\frac{N_1}{105}\right).$$

refractivity as a function of its value at the surface, N_s, has been defined. Near the ground the following empirical relationship between N_s and the difference in refractivity, ΔN, between N_s and N at 1 km above the Earth's surface is valid:

$$\Delta N \text{ (km)} = -7.32 \exp(0.005577 N_s). \tag{3.40}$$

inverting Equation (3.37), we can obtain N_s as a function of the refractory gradient ΔN:

$$N_s = 412.87 \log|\Delta N| - 356.93. \tag{3.41}$$

Figures 3.2 and 3.3 show estimates of N_s for winter afternoons in the northern temperate zone and global variations. Charts similar to Figure 3.2 applicable for high latitudes may be obtained from the appropriate national meteorological departments. Radio-refractivity values at high latitudes are sometimes radically different from those in temperate zones. For example, Fairbanks, Alaska has some of the steepest temperature inversions in the world, causing anomalous refraction on some VHF/UHF radio paths. These effects will be described in Chapters 8 and 9.

3.3.2 Terrain effects

The most obvious feature of the Earth affecting terrestrial radiowave propagation is its curvature. The troposphere of the Earth refracts radiowaves on LOS paths

Downloaded from Cambridge Books Online by IP 141.211.4.224 on Wed Mar 23 15:38:40 GMT 2016.
http://dx.doi.org/10.1017/CBO9780511535758.005
Cambridge Books Online © Cambridge University Press, 2016

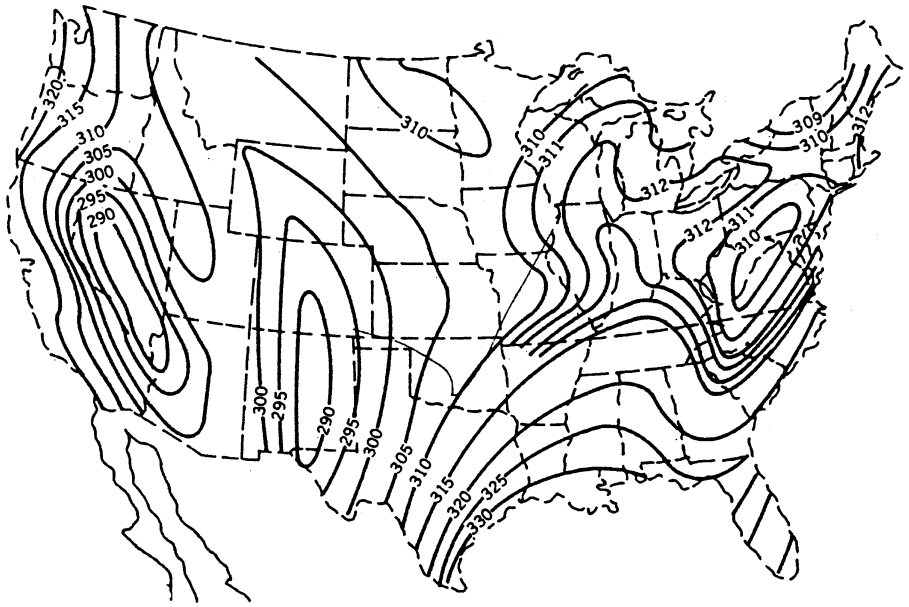

Figure 3.2. Minimum surface-refractivity values (N_s) referred to mean sea level for an average winter afternoon, continental U. S. A. (from Freeman, 1997).

in such a way that one can use a modified Earth-radius when planning these propagation paths and, from Section 3.3.1, we use the "4/3 Earth-curvature" as shown in Figure 3.4.

Topographical features such as mountain ranges and deep valleys will, of course, also affect the propagation of radio waves – especially if they block off low takeoff angles for HF paths or if the ground-reflection areas of a skywave mode occur where are large topographic features. A "rule of thumb" is that the radio horizon should be no higher than about 5° in the desired direction of propagation for a long-haul HF skywave circuit. For LOS propagation, one usually takes advantage of mountains to site either active or passive repeaters for VHF through microwave frequencies.

Theoretical calculations of antenna patterns usually assume that one has a perfectly conducting reflecting plane, when in reality the conductivity and permittivity of the Earth's surface exhibit great variation – as illustrated in Table 3.5. The vertical radiation pattern of a practical antenna depends upon the electrical characteristics of the ground plane of the antenna. For antennas that use the Earth's surface as their ground plane, in addition to the electrical properties of the Earth, the relative "smoothness" of the Earth is also important. The concept of the Fresnel zone is invaluable in calculating the relation of the propagation path to the terrain in the context of engineering the best path characteristics. Extensive treatments of Fresnel zones applied to radio propagation may be found in standard electrical engineering textbooks and Handbooks (see Jordan and Balmain, 1968,

Downloaded from Cambridge Books Online by IP 141.211.4.224 on Wed Mar 23 15:38:40 GMT 2016.
http://dx.doi.org/10.1017/CBO9780511535758.005
Cambridge Books Online © Cambridge University Press, 2016

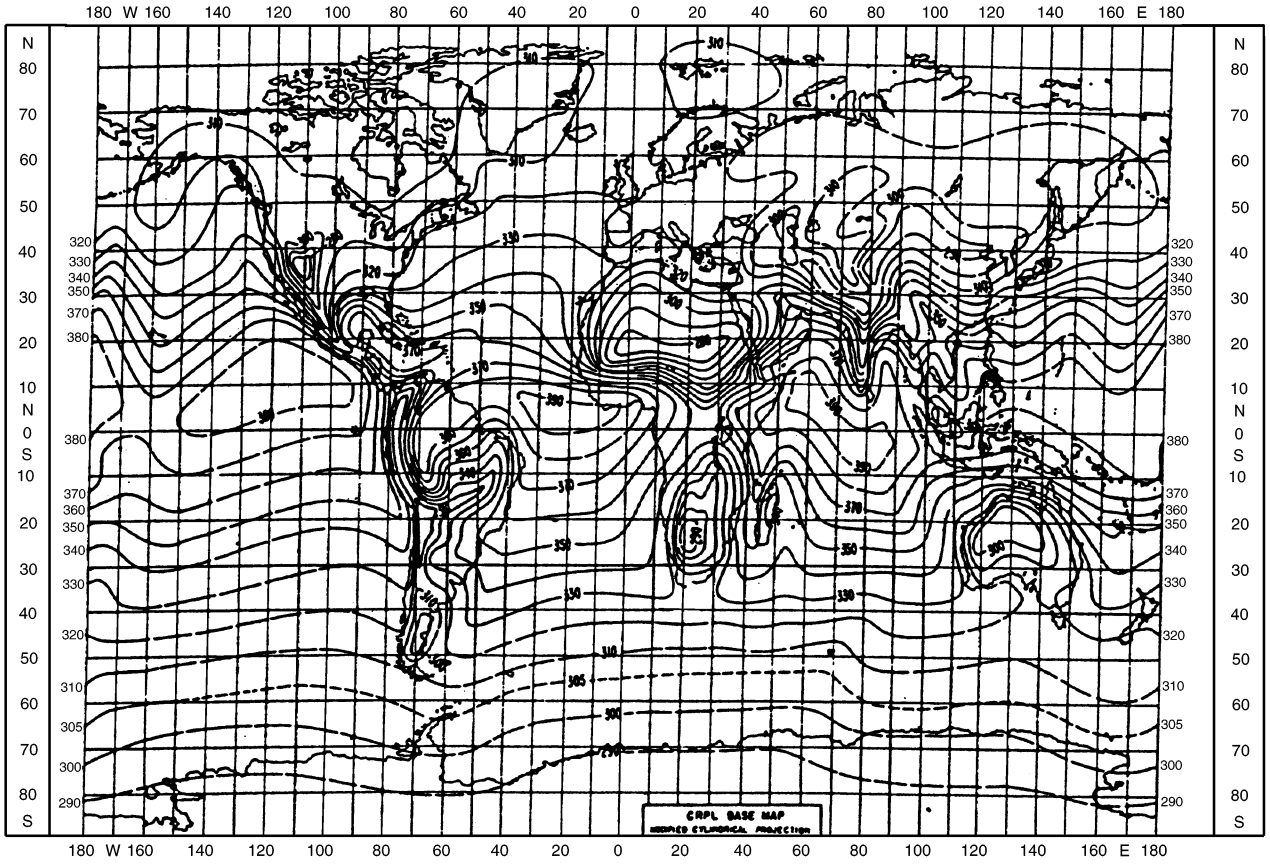

Figure 3.3. Minimum monthly surface-refractivity values (N_s) referred to mean sea level.

Downloaded from Cambridge Books Online by IP 141.211.4.224 on Wed Mar 23 15:38:40 GMT 2016.
http://dx.doi.org/10.1017/CBO9780511535758.005
Cambridge Books Online © Cambridge University Press, 2016

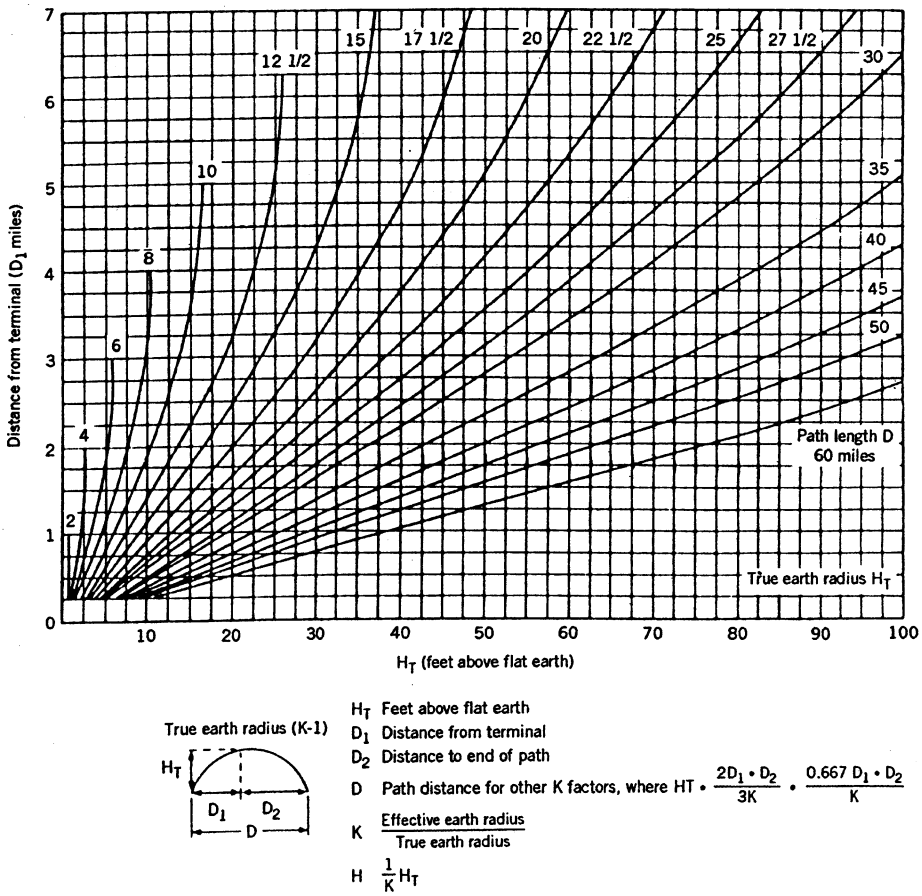

Figure 3.4. Earth-curvature-correction curves for D_1 from 0.5 to 7 miles (from Freeman, 1997).

pp. 498–503; Hall and Barclay, 1989, pp. 38–42 and Hunsucker, 1991, pp. 258–266). Several computer programs which treat terrain effects and LOS link performance have recently become available (Table 3.6). It should also be mentioned that certain atmospheric and ionospheric conditions could produce signals over the LOS distance.

3.3.3 Noise and interference

Electrical noise is one of the limiting factors in radio communication and must be considered in the design of communications circuits. The three components of electrical noise are *cosmic noise*, *atmospheric noise*, and *manmade noise.* There are extensive discussions of the *noise figure* and *noise temperature* of receivers, and cosmic, atmospheric, and manmade noise in Collin (1985), Kraus (1988),

Downloaded from Cambridge Books Online by IP 141.211.4.224 on Wed Mar 23 15:38:40 GMT 2016.
http://dx.doi.org/10.1017/CBO9780511535758.005
Cambridge Books Online © Cambridge University Press, 2016

Spaulding and Washburn (1985), and CCIR Report 322; and a shorter description in Hunsucker (1991, pp. 15–20 and Appendix A5).

Cosmic noise emanates from sources of extraterrestrial origin, such as our Sun, galactic radio sources, and the extragalactic sources, and its dependences on frequency and antenna-pointing direction are shown in Figure 3.5. From Figure 3.5 we see that cosmic radio noise decreases with increasing frequency and varies with the antenna-pointing direction. The terrestrial ionosphere acts as a "high-pass" filter, attenuating or refracting cosmic noise in the ELF through low-HF bands.

Solar radio noise varies in frequency, intensity, and time. An example of the behavior of the *quiet* Sun of large bursts, storms, and plages for frequencies from ~15 MHz to microwave frequencies is shown in Figure 3.6. Good representations of the dynamic behavior of solar radio burst frequency and intensity are shown in Figures 3.7 and 3.8. An example of radio noise from a *galactic* source is shown in Figure 3.9. Examples of the variation with frequency of some *extragalactic* radio sources are illustrated in Figure 3.10.

Atmospheric noise originates in atmospheric electrical discharges like lightning and precipitation static, etc., and may reach the receiving antenna either by a LOS path or via propagation by the ionosphere. The most intense thunderstorms on

Table 3.5. *Electrical conductivities and permitivities for various types of terrain*

Type of surface	Conductivity, σ (Ω^{-1} m^{-1})	Permitivity (ε) (relative dielectric) constant
Coastal dry sand	0.002	10.0
Flat, wet coastal	0.01–0.02	4.0–30.0
Rocky land (steep hills)	0.002	10.0–15.0
Highly moist soil	0.005–0.02	30.0
Marshy	0.1	30.0
Hills (to ~1000 m)	0.001	5.0
Freshwater	0.001	80.0–81.0
Sea water	3.0–5.0	80.0–81.0
Sea ice	0.001	4.0
Polar ice (free)	0.000025	3.0
Polar ice (cap)	0.0001	1.0
Arctic land	0.0005–0.001	23–34 for silts ~12 for dry sand
Tundra underlain by permafrost surface[a]	~10^{-3} to 10^{-2}	~5–70

Note:

[a] Acquired in 1988/1989 in Central Alaska from 2–30 MHz by G. Hagn of SRI International.

Downloaded from Cambridge Books Online by IP 141.211.4.224 on Wed Mar 23 15:38:40 GMT 2016.
http://dx.doi.org/10.1017/CBO9780511535758.005
Cambridge Books Online © Cambridge University Press, 2016

earth occur in the tropics and this HF noise is propagated by LOS modes and by the ionosphere to distances of thousands of kilometers. The areas of *lowest* propagated atmospheric noise are at high northern and southern latitudes (>55° geographic latitude).

Table 3.6. *Computer programs for diffraction/terrain predictions*

Name	Description	Source	Reference
EREPS	Engineer's Refractive Effects Prediction System	http://trout.nosc.mil/NraDMosaicHome.html	Patterson (1994), Proc. of the BLOS Conference
IFDG/GTD	*Finite Difference.../ Generalized Theory of Diffraction		Anderson *et al.* (1993) Marcus (1994)
GELTI/ATLM	GTD Estimated Loss due to Terrain Interaction/ Automated Terrain Linearization Model	Dr Kent Chamberlain Department of Electrical and Computer Engineering, University of New Hampshire, Durham, NH 03824-3591	Chamberlain and Luebbers (1992)
HARPO	Hamiltonian equations in spherical coordinates, modified by using Gaussian beams		Brent and Ormsby (1994)
EFEPE/SSP IRT	Institut für Rundfunktechnik propagation model for digital broadcast systems in urban areas	Dr R. Großkopf Institut für Rundfunktechnik München	Ditto Grosskopf (1994)
VTRPE	Variable Terrain Radio Parabolic Equation microwave propagation in complex real-world environments	Dr Frank Ryan NCCOSC/RDT&E Division, San Diego, CA 92152-6435	Ryan (1991)

Downloaded from Cambridge Books Online by IP 141.211.4.224 on Wed Mar 23 15:38:40 GMT 2016.
http://dx.doi.org/10.1017/CBO9780511535758.005
Cambridge Books Online © Cambridge University Press, 2016

Table 3.6. (*cont.*)

Name	Description	Source	Reference
MSITE, TPATH, MCS	Two- and three-dimensional plots of signal levels from multiple transmitters, microwave-link studies and interference prediction, ray-tracing for urban and indoor environments, wireless, etc.	EDX Engineering, Inc., P. O. Box 1547, Eugene, OR 97440 Ph. (541)345-0019 Fax (541)345-8145 http://www.edx.com	
TIREM/ DUCTAPE	Terrain Integrated Rough-Earth Model/ Ducting and Anomalous Propagation Environment	Dr Homer Riggins and Dr David Eppink, IIT Research Institute, 185 Admiral Cochrane Drive, Annapolis, MD	Eppink and Kuebler (1994)

Several reports and papers deal with the global levels of atmospheric noise, the most cited being Spaulding and Washburn (1985) and the CCIR Report 322-3c (1988). Sailors (1993) has noted some major problems in CCIR Report 322-3, and concludes that "the model should be used with caution, especially in the northern and southern high latitudes, the Arabian Peninsula, northern Africa and the mid-Atlantic areas. In these areas, consider using the original CCIR Report 322 model." He also suggests serious modifications to the development of the model and using correction factors for certain locations. Figures 3.11–3.15 give examples of atmospheric models and noise as a function of frequency.

Manmade noise usually originates from rotating electrical machinery, high-current switching circuits, and arcing power-line components. It is obviously most intense in industrial areas and problems from this type of noise need to be resolved on a case-by-case basis as outlined in a report by Vincent and Munsch (1996).

Interference from other transmitters sometimes dominates portions of the spectrum, such as the HF band – where frequency assignments seem to be largely ignored. Interference can be minimized by maintaining the frequency stability of

Downloaded from Cambridge Books Online by IP 141.211.4.224 on Wed Mar 23 15:38:40 GMT 2016.
http://dx.doi.org/10.1017/CBO9780511535758.005
Cambridge Books Online © Cambridge University Press, 2016

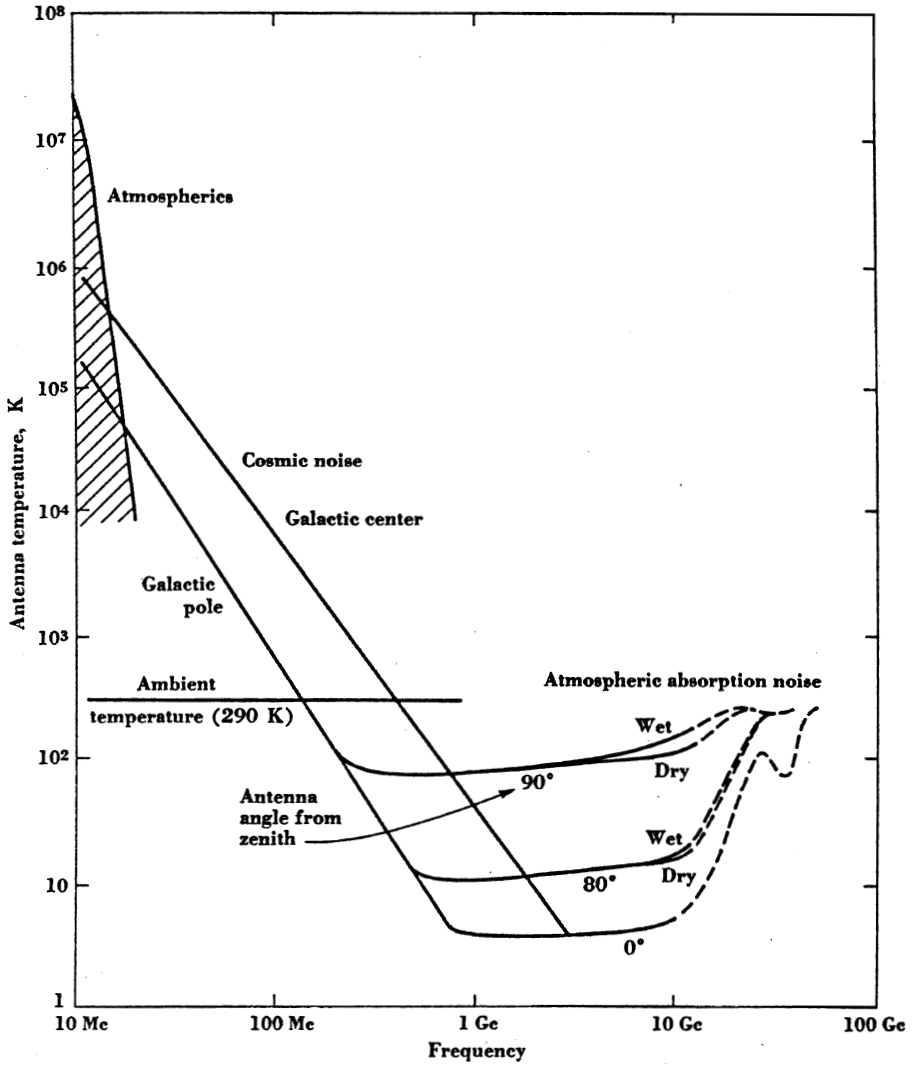

Figure 3.5. Variations of "antenna temperature" as a function of frequency from 10 MHz to 100 GHz (from Freeman, 1997).

the transmitter and maximizing the selectivity of the receiver and by making rather extensive interference measurements at the receiver site before finalizing the operating frequency and time slots.

The basic theorems governing vertical and oblique HF propagation are given in the following section.

Downloaded from Cambridge Books Online by IP 141.211.4.224 on Wed Mar 23 15:38:40 GMT 2016.
http://dx.doi.org/10.1017/CBO9780511535758.005
Cambridge Books Online © Cambridge University Press, 2016

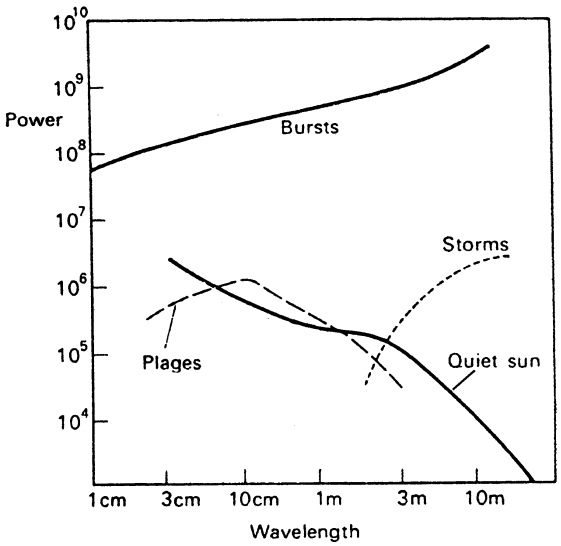

Figure 3.6. A typical radio spectrum from the Sun (after Hey, 1983).

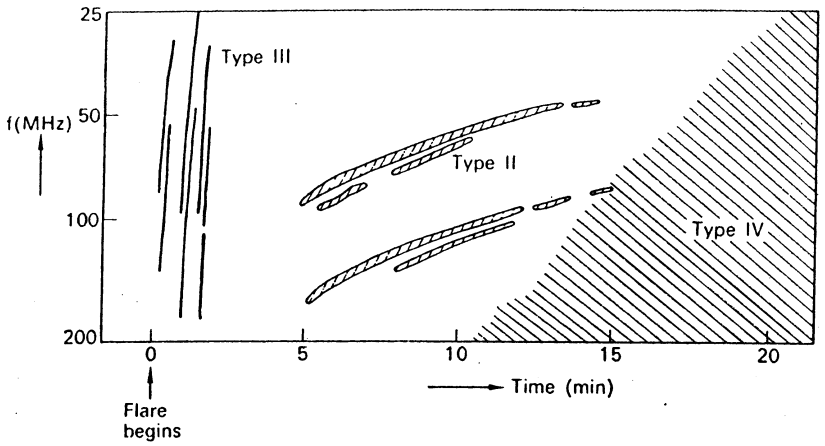

Figure 3.7. Dynamic spectra of solar radio bursts (from Hey, 1983, p. 100).

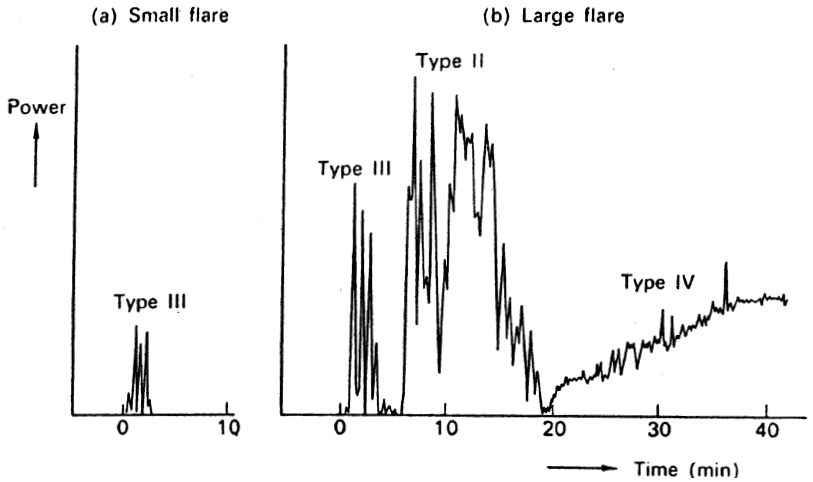

Figure 3.8. The power variation of solar radio bursts (from Hey, 1983, p. 100).

Downloaded from Cambridge Books Online by IP 141.211.4.224 on Wed Mar 23 15:38:40 GMT 2016.
http://dx.doi.org/10.1017/CBO9780511535758.005
Cambridge Books Online © Cambridge University Press, 2016

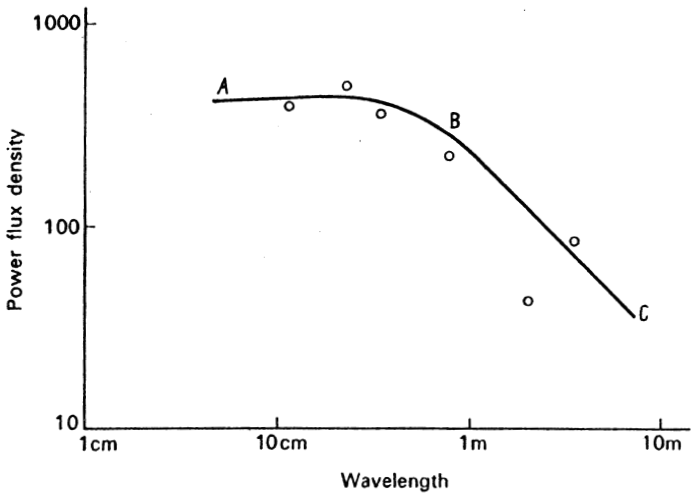

Figure 3.9. The spectrum of radio sources in the Orion Nebula compared with a curve calculated for an electron temperature of 10000 K (from Hey, 1983).

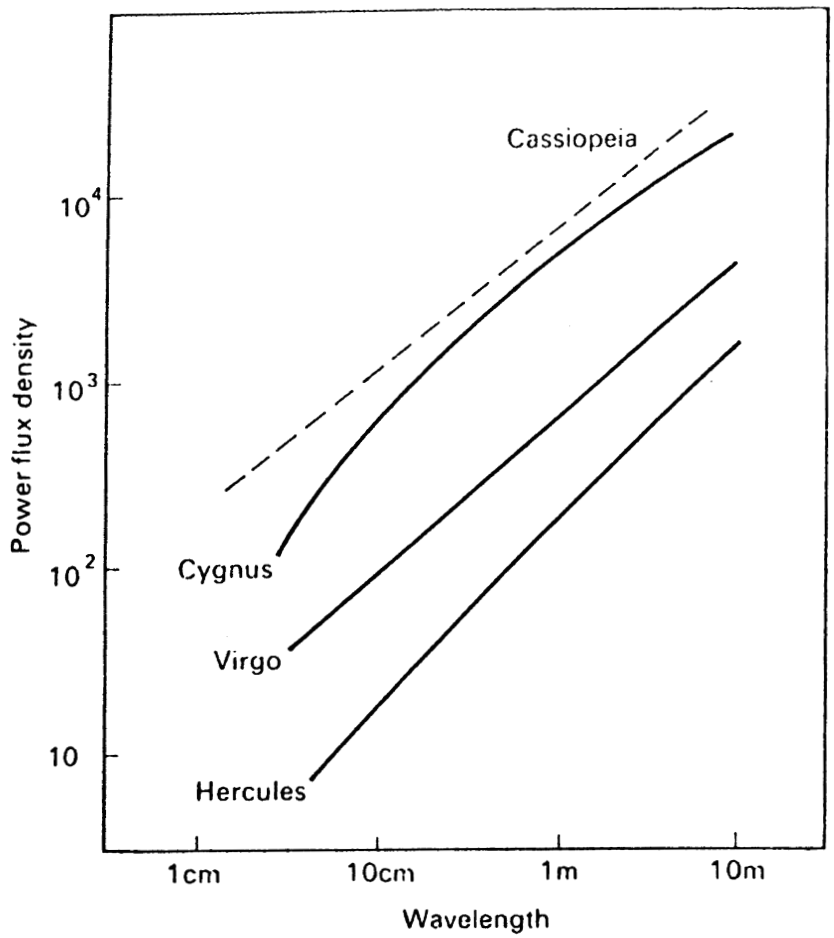

Figure 3.10. Spectra of radio galaxies Cygnus A, Virgo A, and Hercules A, compared with the supernova remnants in Cassiopeia (dashed curve) (from Hey, 1983).

Downloaded from Cambridge Books Online by IP 141.211.4.224 on Wed Mar 23 15:38:40 GMT 2016.
http://dx.doi.org/10.1017/CBO9780511535758.005
Cambridge Books Online © Cambridge University Press, 2016

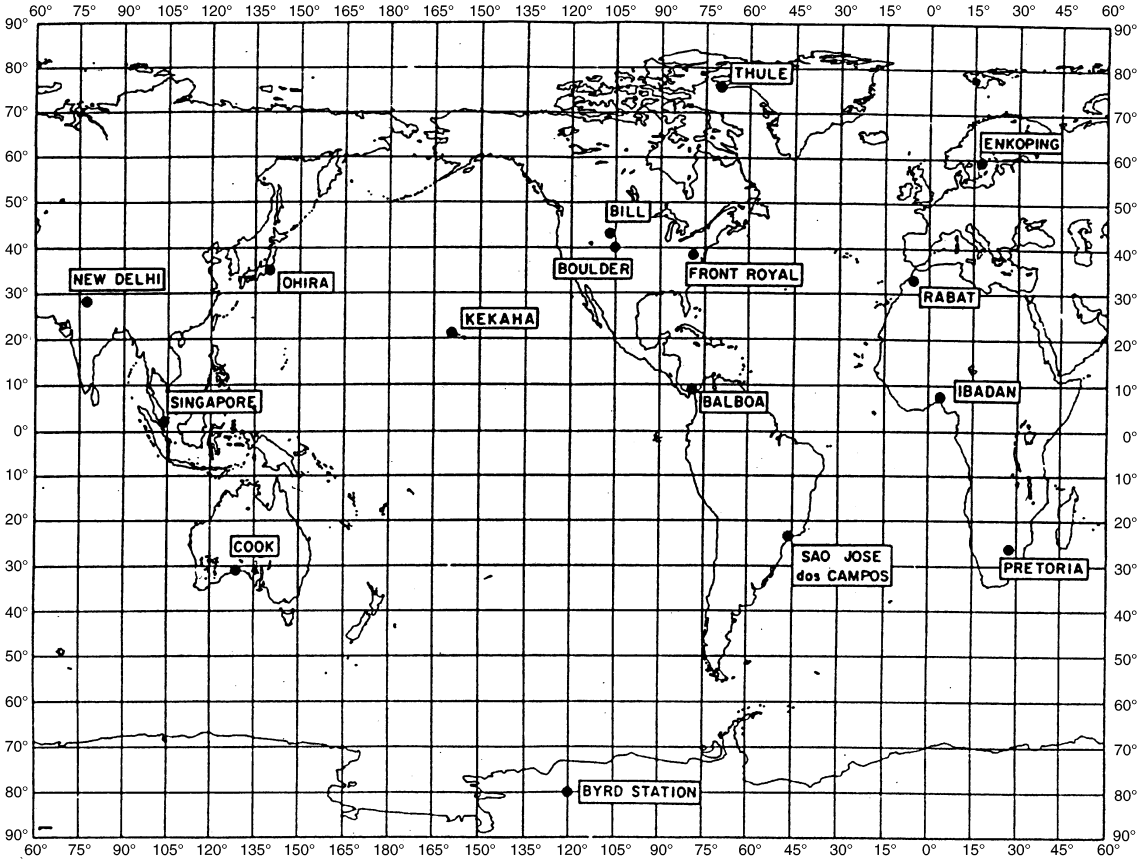

Figure 3.11. Radio-noise-recording stations used to obtain data used to develop the original CCIR Report 322 (from Sailors, 1993).

Downloaded from Cambridge Books Online by IP 141.211.4.224 on Wed Mar 23 15:38:40 GMT 2016.
http://dx.doi.org/10.1017/CBO9780511535758.005
Cambridge Books Online © Cambridge University Press, 2016

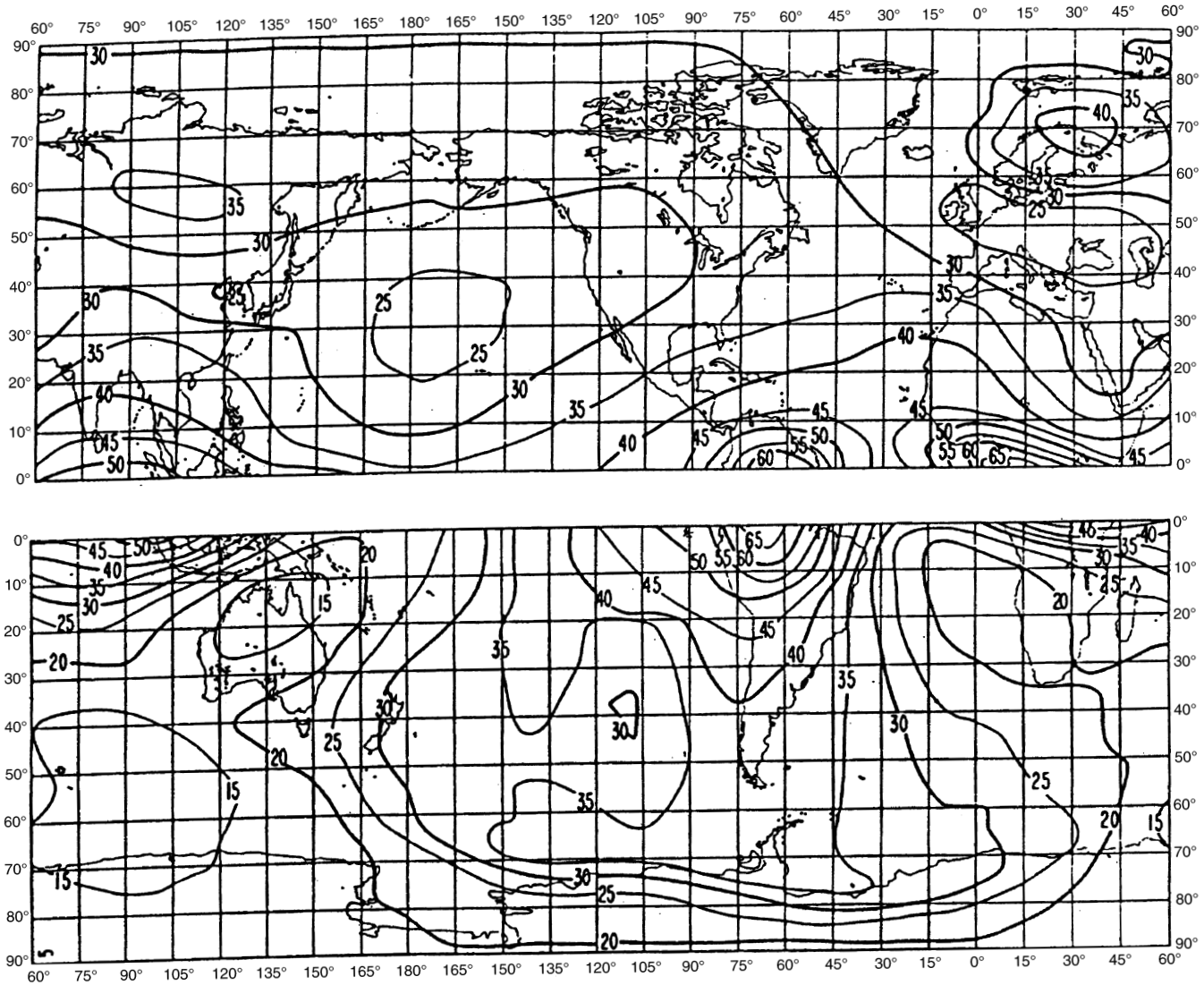

Figure 3.12. A typical figure from CCIR Report 322 (from Sailors, 1993).

Downloaded from Cambridge Books Online by IP 141.211.4.224 on Wed Mar 23 15:38:40 GMT 2016.
http://dx.doi.org/10.1017/CBO9780511535758.005
Cambridge Books Online © Cambridge University Press, 2016

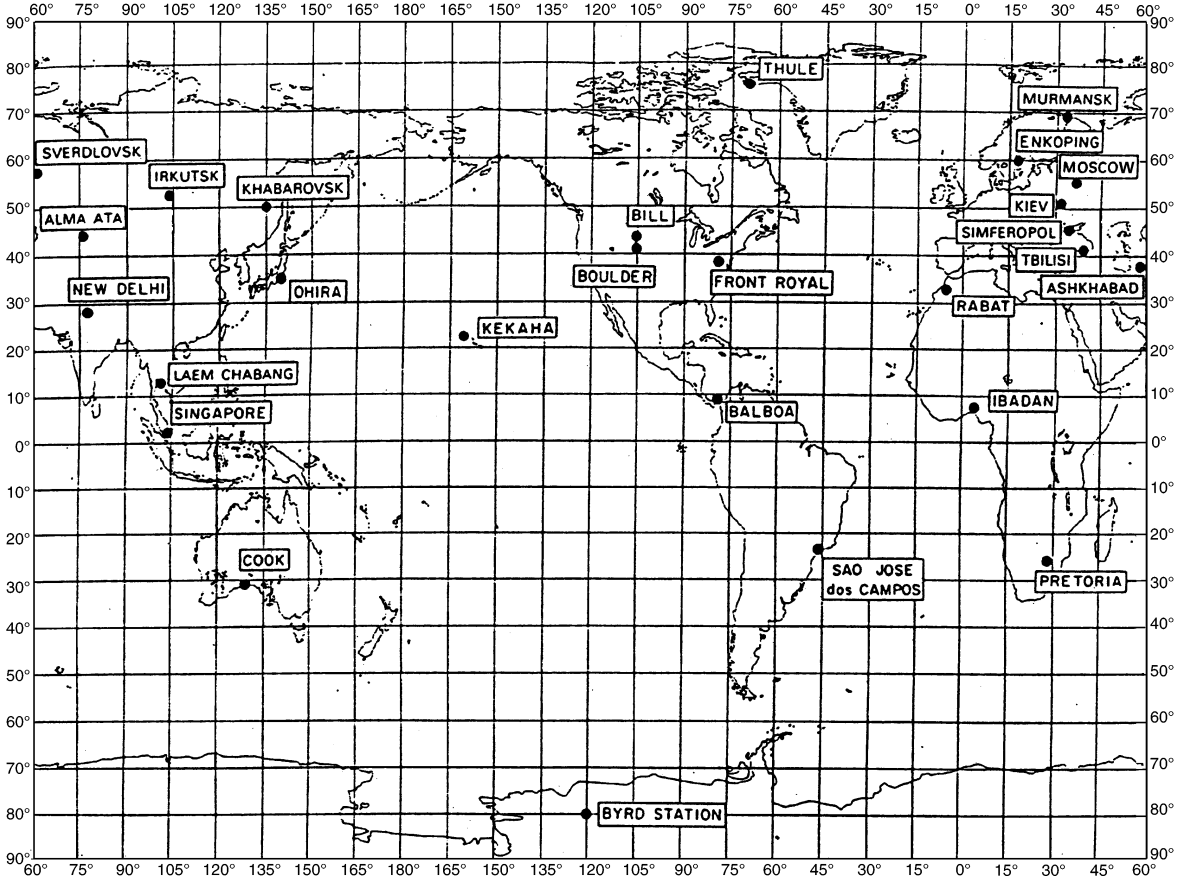

Figure 3.13. Radio-noise-recording locations (from Sailors, 1993).

Downloaded from Cambridge Books Online by IP 141.211.4.224 on Wed Mar 23 15:38:40 GMT 2016.
http://dx.doi.org/10.1017/CBO9780511535758.005
Cambridge Books Online © Cambridge University Press, 2016

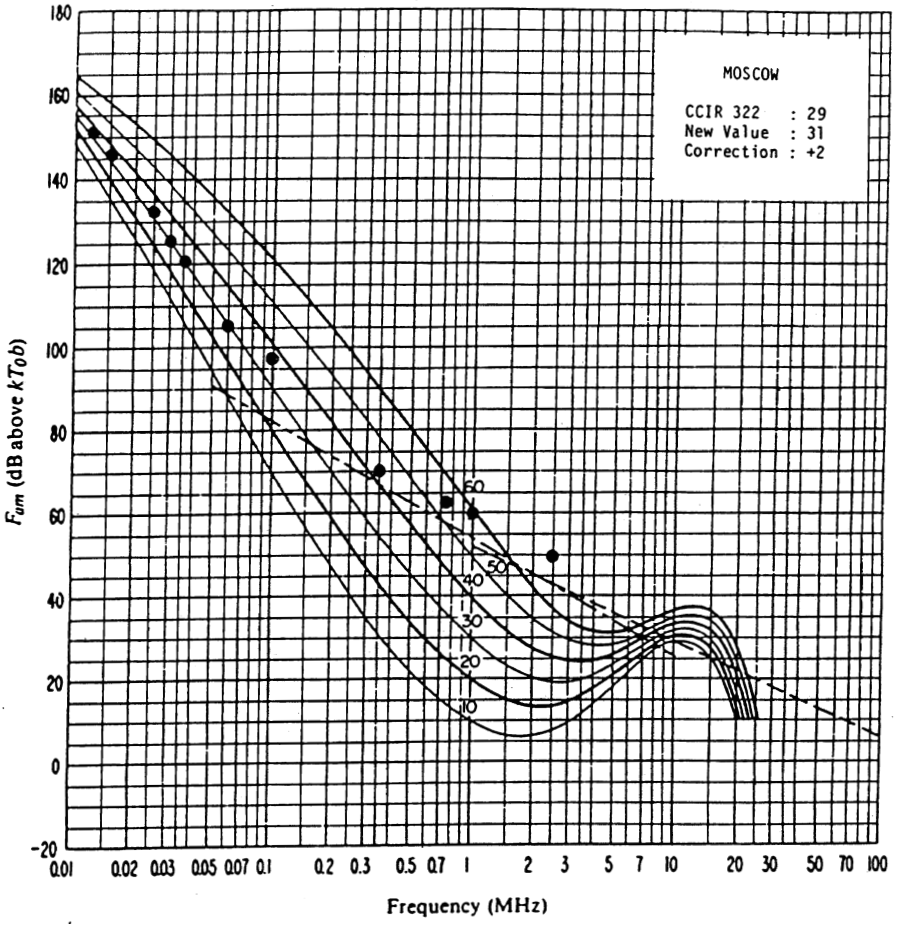

Figure 3.14. Determination of the 1-MHz F_{am} value for Moscow for June, July and August; 1600–2000 UT. (from Spaulding and Washburn, 1985).

Downloaded from Cambridge Books Online by IP 141.211.4.224 on Wed Mar 23 15:38:40 GMT 2016.
http://dx.doi.org/10.1017/CBO9780511535758.005
Cambridge Books Online © Cambridge University Press, 2016

(a)

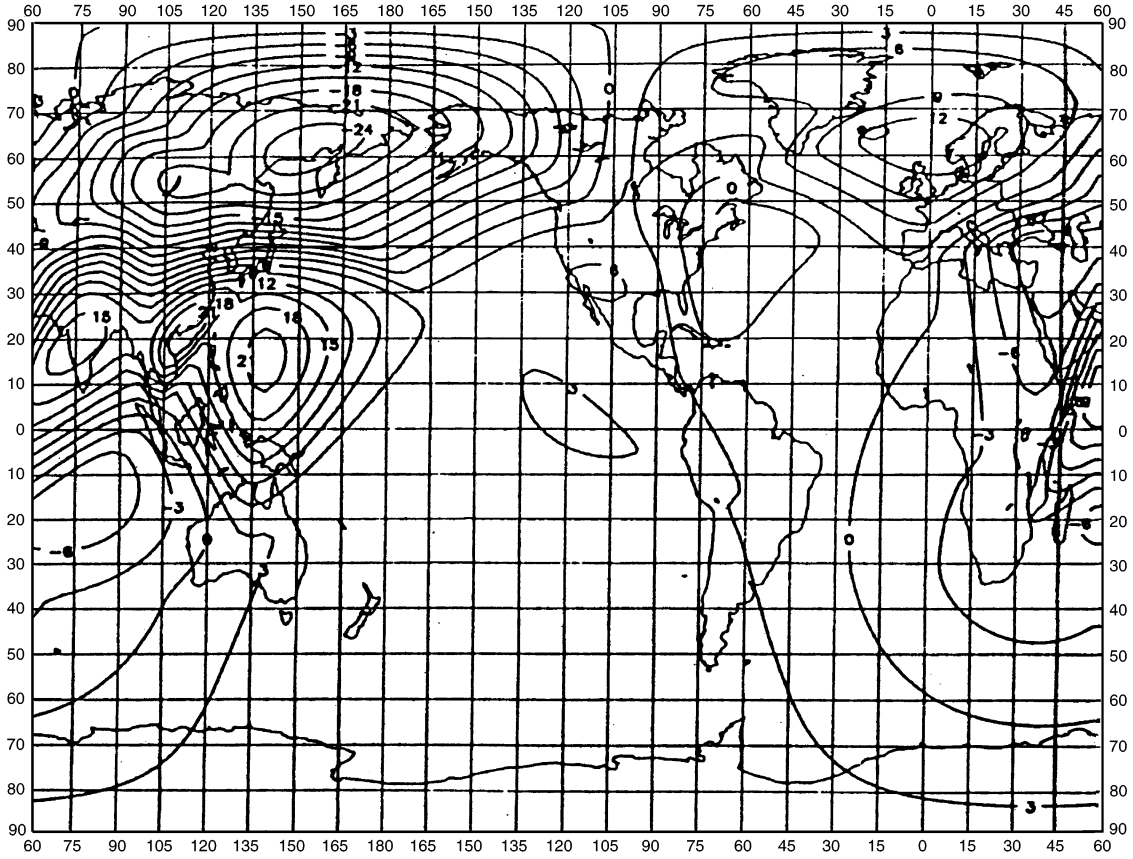

Downloaded from Cambridge Books Online by IP 141.211.4.224 on Wed Mar 23 15:38:40 GMT 2016.
http://dx.doi.org/10.1017/CBO9780511535758.005
Cambridge Books Online © Cambridge University Press, 2016

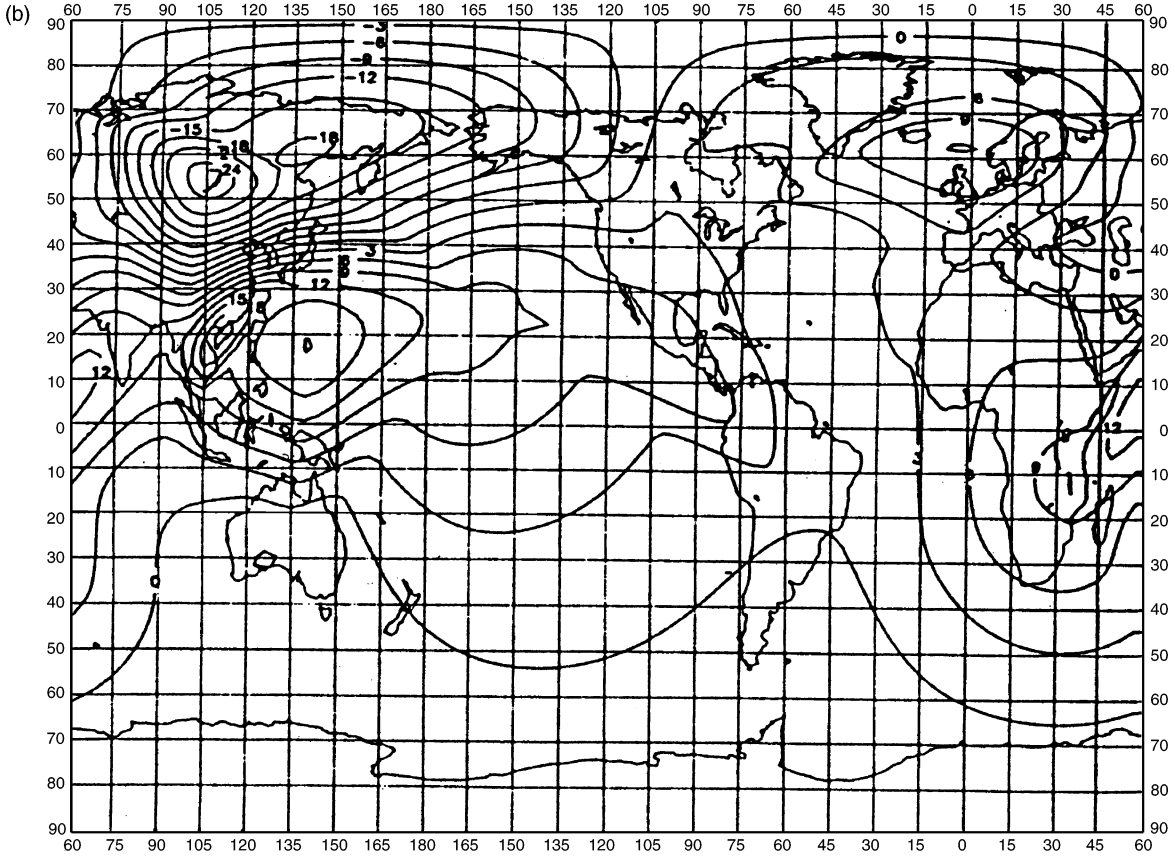

Figure 3.15. In (a) and (b) are shown examples of Spaulding and Washburn's corrections to the CCIR Report 322 (from Spaulding and Washburn, 1985, p. 18).

Downloaded from Cambridge Books Online by IP 141.211.4.224 on Wed Mar 23 15:38:40 GMT 2016.
http://dx.doi.org/10.1017/CBO9780511535758.005
Cambridge Books Online © Cambridge University Press, 2016

3.4 Ionospheric propagation

3.4.1 Magnetoionic theory

The Appleton equation

For an ionized medium the refractive index is expressed by the Appleton equation. In its complete form this is a complicated expression using the dimensionless quantities X, Y, and Z, each of which is defined as a ratio between the wave frequency and a frequency characteristic of the medium. The latter are the *plasma frequency*,

$$\omega_N = [Ne^2/\varepsilon_0 m_e]^{1/2}, \tag{3.42}$$

the *gyrofrequency*,

$$\omega_B = Be/m_e, \tag{3.43}$$

and the *collision frequency*, ν, where N is the electron concentration (usually called the *electron density*), e is the charge on the electron (taken to be positive), m_e is the mass of the electron, ε_0 is the permittivity of free space, and B is the magnetic flux density in the medium. The plasma frequency is the natural frequency of oscillation for electrostatic perturbations within the plasma, the gyrofrequency is the frequency of gyration of an electron in magnetic flux density B, and ν is the rate of collision between a given electron and other particles. Then the dimensionless quantities are

$$X = \omega_N^2/\omega^2, \tag{3.44}$$

$$Y = \omega_B/\omega, \tag{3.45}$$

and

$$Z = \nu/\omega. \tag{3.46}$$

In these terms the Appleton equation for the refractive index (n) of an ionized medium with N electrons cm^{-3}, permeated by a magnetic flux density B (W m^{-1}) and in which the electron-collision frequency is ν (s^{-1}) is given by

$$n^2 = 1 - \frac{X}{1 - jZ - \dfrac{Y_T^2}{2(1 - X - jZ)} \pm \left(\dfrac{Y_T^4}{4(1 - X - jZ)^2} + Y_L^2 \right)^{1/2}}, \tag{3.47}$$

where + denotes the ordinary and − the extraordinary wave. In (3.47), Y has been divided into longitudinal and transverse components;

Downloaded from Cambridge Books Online by IP 141.211.4.224 on Wed Mar 23 15:38:40 GMT 2016.
http://dx.doi.org/10.1017/CBO9780511535758.005
Cambridge Books Online © Cambridge University Press, 2016

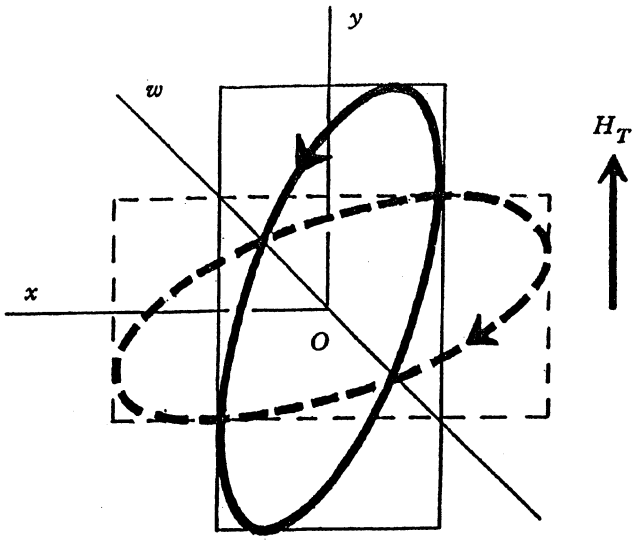

Figure 3.16. The electric-field polarization in the plane of the wavefront. Ox and Oy are the principal directions and the projection of the imposed magnetic field is along Oy. The positive wave-normal is directed into the paper, along positive Oz. The ordinary-wave ellipse is shown as a continuous line and the extraordinary-wave ellipse is shown as a dashed line (from Ratcliffe, 1959).

$$Y_{\mathrm{L}} = Y\cos\theta \tag{3.48a}$$

and

$$Y_{\mathrm{T}} = Y\sin\theta, \tag{3.48b}$$

θ being the angle between the direction of propagation and the magnetic field. Note that the refractive index is complex, with real and imaginary parts: $n = \mu - \mathrm{j}\chi$.

Polarization

In order to calculate the effects of this anisotropic medium on the *polarization* of a radio wave traversing the region, it is convenient to define the polarization ratio R as

$$R = -H_y/H_x = E_x/E_y, \tag{3.49}$$

where H_y and E_y are the y-components of **E** and **H**, and H_x and E_x are the x-components of **E** and **H**, respectively. Then we can obtain the *magnetoionic polarization equation* (see Kelso, 1964; and Ratcliffe, 1959)

$$R = -\frac{\mathrm{j}}{Y_{\mathrm{L}}}\left[\frac{Y_{\mathrm{T}}^2}{2(1-X-\mathrm{j}Z)} \mp \left(\frac{Y_{\mathrm{T}}^4}{4(1-X-\mathrm{j}Z)^2} + Y_{\mathrm{L}}^2\right)^{1/2}\right]. \tag{3.50}$$

The polarization equation gives values of R that are complex. In general, this means an elliptical polarization. If R is purely real, the polarization is linear; if R is purely imaginary, the polarization is circular. See Figure 3.16.

Downloaded from Cambridge Books Online by IP 141.211.4.224 on Wed Mar 23 15:38:40 GMT 2016.
http://dx.doi.org/10.1017/CBO9780511535758.005
Cambridge Books Online © Cambridge University Press, 2016

It is virtually impossible for an ordinary mortal to make much sense of Equations (3.47) and (3.50) in their full glory – see Ratcliffe (1959) or Budden (1985) for a full discussion – but when special cases are taken the picture begins to clarify. Luckily, many applications can be treated using these special cases.

Special case 1: Neglecting collisions and magnetic field

If there are no collisions and the magnetic field is neglected, the refractive index, n, is real:

$$\begin{aligned} n^2 &= 1 - \mathrm{X} = 1 - \omega_N^2/\omega^2 \\ &= 1 - Ne^2/(\varepsilon_0 m_\mathrm{e}\omega^2). \end{aligned} \tag{3.51}$$

Then the phase velocity is

$$v_\mathrm{p} = c/n = c\left/\left(1 - \frac{Ne^2}{\varepsilon_0 m_\mathrm{e}\omega^2}\right)^{1/2}\right. . \tag{3.52}$$

The group velocity, using Equation 3.21, is

$$u = c/n_\mathrm{g} = c\left(1 - \frac{Ne^2}{\varepsilon_0 m_\mathrm{e}\omega^2}\right)^{1/2}, \tag{3.53}$$

where n_g is the group refractive index. (Note that $n_\mathrm{g} = 1/n$ in this case.)

Special case 2: The effect of a magnetic field

If the magnetic field is now included and the propagation is almost directly along the magnetic vector so that Y_T may be neglected, then

$$\begin{aligned} n^2 &= 1 - X/(1 \pm Y_\mathrm{L}) \\ &= 1 - \omega_N^2/[\omega(\omega \pm \omega_\mathrm{L}) \end{aligned} \tag{3.54}$$

and $R = \pm \mathrm{j}$. There are now two waves, circularly polarized in opposite directions, having different velocities. These are *characteristic waves,* termed *ordinary* and *extraordinary* (for the upper and lower signs, respectively) by analogy with birefringence in crystals. In general, where $Y_\mathrm{T} \neq 0$, the characteristic waves are elliptically polarized.

Special case 3: The effect of collisions

If collisions are significant (but in the absence of a magnetic field), then

$$\begin{aligned} n^2 &= 1 - X/(1 - \mathrm{j}Z) \\ &= 1 - \omega_N^2/[\omega(\omega - \mathrm{j}\nu)]. \end{aligned} \tag{3.55}$$

Downloaded from Cambridge Books Online by IP 141.211.4.224 on Wed Mar 23 15:38:40 GMT 2016.
http://dx.doi.org/10.1017/CBO9780511535758.005
Cambridge Books Online © Cambridge University Press, 2016

Taking the imaginary part (χ) and applying Equation (3.25) gives the absorption coefficient

$$\kappa = \frac{\omega}{c}\frac{1}{2\mu}\frac{XZ}{1+Z^2}$$

$$= \frac{e^2}{2\varepsilon_0 m_e c}\frac{1}{\mu}\frac{N\nu}{\omega^2+\nu^2}. \tag{3.56}$$

The refractive index (n) is modified by collisions between the electrons and heavy particles, and the wave undergoes absorption – which physically is due to the conversion of ordered momentum into random motion of the particles after collision. At each collision, some energy is transferred from the wave to the neutral molecules and appears as *thermal energy*. Details of the *microscopic* processes involved in ionospheric absorption are discussed by Ratcliffe (1959, Ch. 5) and derivations of the equations describing *macroscopic* features of absorption are given by Davies (1969, Ch. 6).

We can conveniently divide absorption into two limiting types, commonly called *non-deviative* absorption and *deviative* absorption. Non-deviative absorption occurs in regions where the product $N\nu$ is large and $\mu \approx 1$, and is characterized by the absorption of LF, MF, and HF waves in the D region. Deviative absorption, on the other hand, occurs near the top of the ray trajectory or anywhere else on the ray path where significant bending takes place (for small $N\nu$ and μ).

When the refractive index is ≈ 1, we can write

$$\kappa = 4.6\times 10^{-2}\frac{N\nu}{\omega^2+\nu^2}\ (\text{dB km}^{-1}). \tag{3.57}$$

We can further simplify Equation (3.57) for the VHF case, since $\omega^2 \gg \nu^2$, as

$$\kappa = 4.6\times 10^{-2} N\nu/\omega^2\ (\text{dB km}^{-1}). \tag{3.58}$$

In deviative absorption, $\mu < 1$, and

$$\kappa \approx \frac{\nu}{2c\mu}(1-\mu^2). \tag{3.59}$$

Near a reflection level, $\mu^2 \ll 1$, and then the preceding equation reduces to

$$\kappa \approx \frac{\nu}{2c}\mu', \tag{3.60}$$

where μ' is the group refractive index.

One important case is for non-deviative absorption and the quasi-longitudinal (QL) approximation, when

Downloaded from Cambridge Books Online by IP 141.211.4.224 on Wed Mar 23 15:38:40 GMT 2016.
http://dx.doi.org/10.1017/CBO9780511535758.005
Cambridge Books Online © Cambridge University Press, 2016

$$\kappa \approx \frac{e^2}{2\varepsilon_0 mc} \frac{N\nu}{(\omega \pm \omega_L)^2 + \nu^2}. \tag{3.61}$$

The absorption coefficient is therefore smaller for the ordinary than it is for the extraordinary wave. For a given value of the electron density, the absorption coefficient is a maximum at the level where

$$\nu = \omega \pm \omega_L. \tag{3.62}$$

The absorption of the extraordinary wave becomes very strong at the higher levels (ν small) when the wave frequency is close to the gyrofrequency.

3.4.2 Reflection of radio waves from an ionospheric layer

Reflection at vertical incidence

If a pulse of radio waves of frequency $f = \omega/(2\pi)$ enters an ionospheric layer at vertical incidence from below, it will travel at the group velocity (u). Neglecting the magnetic field, u is given by Equation (3.53) and u decreases as the electron density increases with altitude. Provided that the layer is sufficiently intense, a level where the group velocity is zero (and the phase velocity infinite) will eventually be reached, and here the energy is reflected. At this level the plasma frequency ($f_N = \omega_N/(2\pi)$) equals the wave frequency (f) and

$$N = 4\pi^2 \varepsilon_0 m_e f_N^2 / e^2. \tag{3.63}$$

Numerically,

$$N\,(\mathrm{m}^{-3}) = 1.24 \times 10^{10} [f\,(\mathrm{MHz})]^2. \tag{3.64}$$

Above this level the wave is evanescent (Equation (3.32)).

The time required for the journey to the reflection point and back is

$$t = \frac{2}{c} \int_0^h \frac{\mathrm{d}z}{n} \tag{3.65}$$

and the *virtual height* is

$$h' = \frac{ct}{2} = \int_0^h \frac{\mathrm{d}z}{[1 - (f_n/f)^2]^{1/2}}. \tag{3.66}$$

The virtual height is the height calculated on the assumption that the signal traveled at the speed of light (*in vacuo*). In fact, since the pulse always travels more slowly in the layer, the virtual height is always greater than the *true height*.

If the electron density at the layer maximum is N_{max}, the greatest radio fre-

Downloaded from Cambridge Books Online by IP 141.211.4.224 on Wed Mar 23 15:38:40 GMT 2016.
http://dx.doi.org/10.1017/CBO9780511535758.005
Cambridge Books Online © Cambridge University Press, 2016

quency that may be reflected at vertical incidence is the *critical frequency of the layer*, f_c, which is related to the maximum electron density by

$$N_{max} = 1.24 \times 10^{10} f_c^2. \tag{3.67}$$

A good discussion of the solution of Abel's equation (3.66) (Appleton, 1930) is given by Kelso (1964). In the general case (including the geomagnetic field), several numerical techniques have been employed successfully to invert the ionogram trace of the ordinary wave to give an equivalent monotonic electron-density profile (see the special issue of *Radio Science*, 1967). One of the most comprehensive of the numerical true height programs is the POLAN program developed by Titheridge (1985) and a discussion of this program is given by Davies (1990).

In the real ionosphere, where the geomagnetic field has to be taken into account, there are two reflection conditions. The *extraordinary wave* is reflected where

$$f_N^2 = f(f - f_B) \tag{3.68}$$

and the *ordinary wave* where

$$f_N = f. \tag{3.69}$$

The first reflection occurs according to the QL approximation, whereas the second relates to the quasi-transverse (QT) approximation. If $f_B \ll f_N$, the difference between the two critical frequencies is $f_B/2$, that for the extraordinary wave being the greater.

3.4.3 Relations between oblique and vertical incidence

When the signal is incident obliquely on the layer, the process by which it is returned to the ground can be appreciated as follows. Consider the ionospheric layer to be composed of a large number of thin, uniform slabs, whose electron density increases with altitude. If successive slabs have refractive indices n_1 and n_2, Snell's law relates the angles of incidence (ϕ_1) and refraction (ϕ_2) by

$$n_1 \sin \phi_1 = n_2 \sin \phi_2. \tag{3.70}$$

Applying this law to each boundary in turn readily shows that, if a ray enters the ionosphere at incidence ϕ_0, its angle to the normal in a slab with refractive index n_r is simply

$$\sin \phi_r = \sin \phi_0 / n_r \tag{3.71}$$

Downloaded from Cambridge Books Online by IP 141.211.4.224 on Wed Mar 23 15:38:40 GMT 2016.
http://dx.doi.org/10.1017/CBO9780511535758.005
Cambridge Books Online © Cambridge University Press, 2016

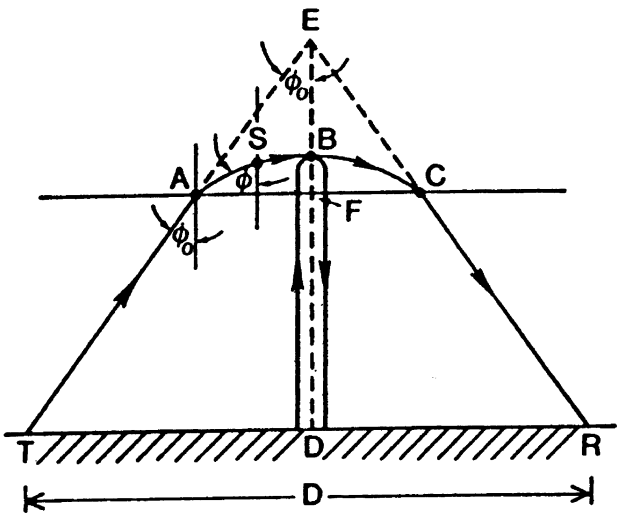

Figure 3.17. The geometry describing vertical and oblique ionospheric propagation (from Hunsucker, 1992).

(the refractive index below the layer being unity). The ray therefore travels horizontally when

$$n_r = \sin\phi_0 \tag{3.72}$$

and this is the reflection condition (magnetic field neglected) for an obliquely incident signal. The ray then returns to the ground by a similar path. The process is now one of bending rather than reflection at a boundary.

Combining the two equations for f_N in this section yields the *secant law* relating vertical and oblique propagation:

$$f_{ob} = f_v \sec\phi_0 \tag{3.73}$$

where f_{ob} and f_v are the frequencies of signals reflected from the same true height when f_{ob} is incident at angle ϕ_0 and f_v is incident vertically.

In order to determine values of $\sec\phi_0$ and f_{ob} from vertical-incidence soundings (which measure the virtual height, h'), we need the results of two more theorems. *Breit and Tuve's* theorem states that the time taken to traverse the actual curved path TABCR in Figure 3.17 at the group velocity u equals the time necessary to travel over the straight-line path TER at the free-space velocity c. Referring to the geometry shown in Figure 3.17, we can write the expression

$$t = \frac{1}{c}\int_{TER} \frac{dx}{\sin\phi_0} \tag{3.74}$$

$$= \frac{D}{c \sin a_0}$$

$$= (TE + ER)/c. \tag{3.75}$$

Downloaded from Cambridge Books Online by IP 141.211.4.224 on Wed Mar 23 15:38:40 GMT 2016.
http://dx.doi.org/10.1017/CBO9780511535758.005
Cambridge Books Online © Cambridge University Press, 2016

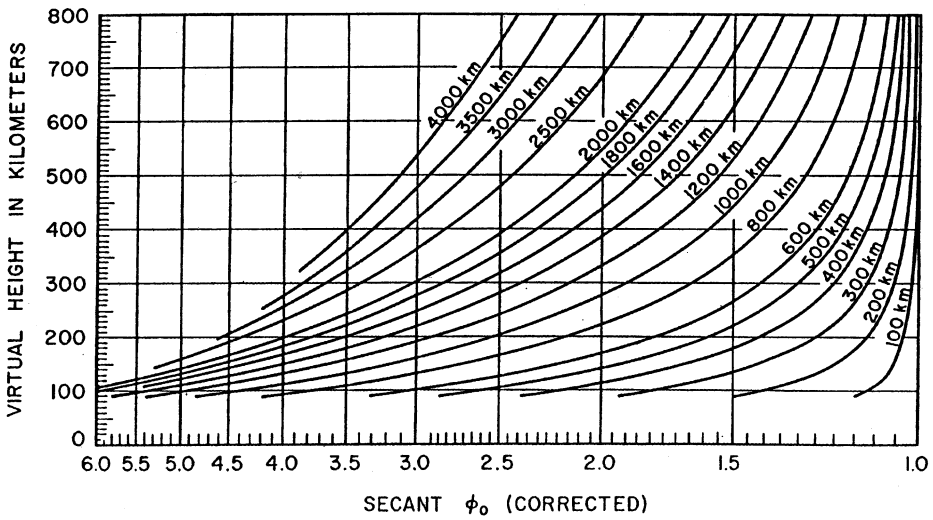

Figure 3.18. Logarithmic ionospheric-transmission curves for a curved-Earth ionosphere (after Smith, 1939).

Martyn's theorem states that, if f_v and f_{ob} are the vertical and oblique frequencies respectively, reflected from the same true height (h), then the virtual height at which the frequency f_{ob} is reflected equals the height of the equivalent triangular path for the frequency f_v. Referring to Figure 3.17 and defining the equivalent path at oblique incidence for frequency f_{ob} as

$$P'_{ob} = 2\mathrm{TE}, \tag{3.76}$$

we obtain

$$P'_v = \cos\phi_0 P'_{ob} = 2\mathrm{DE} \tag{3.77}$$

Martyn's theorem may be written more concisely as

$$\mathrm{h}'_{ob} = \mathrm{h}'_v. \tag{3.78}$$

Newbern Smith (1939) devised the set of logarithmic transmission curves parametric in range for curved Earth shown in Figure 3.18, which are sufficiently accurate for the distances shown. Details concerning the use of these curves to relate the parameters given in Equations (3.76)–(3.78) may be found in Davies (1969) and in the URSI Handbook of Ionogram Analysis (1972).

3.4.4 Trans-ionospheric propagation

If the radio frequency exceeds the critical frequency of the ionosphere, the signal is not reflected but continues out into space. Similarly, signals from beyond the

Downloaded from Cambridge Books Online by IP 141.211.4.224 on Wed Mar 23 15:38:40 GMT 2016.
http://dx.doi.org/10.1017/CBO9780511535758.005
Cambridge Books Online © Cambridge University Press, 2016

ionosphere may be received at the ground if their frequencies are sufficiently high. However, these signals are not necessarily unaffected by the ionosphere: there can be significant and measurable effects on their phase, their polarization and their intensity. In each case the effect becomes weaker with increasing frequency, and in practice they are significant from the upper part of the HF band, through the VHF band, and into the lower part of the UHF band. Another common feature is that the effects are cumulative and the total depends on an integral along the propagation path.

Phase effects

In the Appleton equation for the refractive index, let $X \ll 1$ (radio frequency large relative to the plasma frequency), $Y_L = Y_T = 0$ (geomagnetic field neglected), and $Z = 0$ (collisions neglected). Then the second term of Equation (3.47) is much less than unity, and we can write

$$\begin{aligned} n &= 1 - X/2 \\ &= 1 - Ne^2/(2\varepsilon_0 m_e \omega^2). \end{aligned} \tag{3.79}$$

Inserting values for the constants, and using f instead of ω, gives

$$\mathrm{n} = 1 - 40.30\mathrm{N}\ (\mathrm{m}^{-3})/[f\ (\mathrm{Hz})]^2. \tag{3.80}$$

The refractive index is smaller than unity by an amount proportional to the electron density and inversely proportional to the square of the radio frequency.

If a radio wave travels a distance $\mathrm{d}l$ in an ionized medium, i.e. $\mathrm{d}l/\lambda$ wavelengths, its phase lags by $2\pi \mathrm{d}l/\lambda = (2\pi f \mathrm{n}\, \mathrm{d}l/c)$ radians. Over a path l the advance of phase is therefore

$$-\frac{2\pi f}{c}\int n\,\mathrm{d}l = -\frac{2\pi f l}{c} + \frac{2\pi \times 40.30}{cf}\int N\,\mathrm{d}l. \tag{3.81}$$

The first term is just the phase delay due to a wave of frequency f traveling a distance l at the speed of light. The second is a phase advance that arises because the refractive index is less than unity and the phase speed greater than c. This term is cumulative and simply proportional to the *electron content*, $I = \int N\,\mathrm{d}l$, which is the number of electrons in a column of unit cross-section along the propagation path. Numerically, the phase advance due to the medium is

$$\phi = (8.45 \times 10^{-7}) I/f\ (\text{radians}). \tag{3.82}$$

f is in hertz and I in m^{-2}.

Downloaded from Cambridge Books Online by IP 141.211.4.224 on Wed Mar 23 15:38:40 GMT 2016.
http://dx.doi.org/10.1017/CBO9780511535758.005
Cambridge Books Online © Cambridge University Press, 2016

Several significant applications follow.

(a) Since the phase advance depends upon the radio frequency, the electron content can be determined by comparing the effects on two frequencies transmitted coherently from, for example, a satellite.

(b) Since the frequency is the rate of change of phase, another method is to observe the Doppler shift in the frequency of a signal received from a satellite passing overhead.

(c) If a carrier of frequency f_c is modulated at frequency f_m, the phase of the modulation is changed by

$$\phi_m = -8.45 \times 10^{-7} (f_m / f_c^2) I. \tag{3.83}$$

In this case the phase is retarded because the modulation travels at the group speed, which is less than the speed of light.

(d) Corresponding to this phase delay, the time delay of a pulse is

$$\Delta t = 8.45 \times 10^{-7} I / (2\pi f_c^2) \text{ (s)}. \tag{3.84}$$

(e) If there is a gradient of electron content in a direction (x) perpendicular to the propagation direction, the ray is deviated. This is *wedge refraction*. The wave is deviated through an angle

$$\alpha = [c/(2\pi)](8.45 \times 10^{-7} / f^2)\, \delta I / \delta x. \tag{3.85}$$

(In Equations (3.82)–(3.85) the constant 8.45×10^{-7} is given to three significant figures, therefore with an inaccuracy of 0.12%. To four figures, for more accurate work, the constant is 8.448×10^{-7}. In Equation (3.81) the constant 40.30 is accurate to within 0.025%. To five figures this constant is 40.302).

The Faraday effect

When the geomagnetic field is taken into account and propagation is almost along the field direction, there are two characteristic waves that travel at different speeds. These waves are circularly polarized in opposite directions, and their sum is a linear polarization. If the circularly polarized components make instantaneous angles θ_O and θ_E with respect to a reference direction, then the linear wave is at an angle

$$\Omega = (\theta_O + \theta_E)/2. \tag{3.86}$$

See Figure 3.19.

Let $\theta_O = \theta_E = 0$ at the source. Then, after a distance l in the medium,

$$\theta_O = 2\pi f [t + n_O l / c]$$

Downloaded from Cambridge Books Online by IP 141.211.4.224 on Wed Mar 23 15:38:40 GMT 2016.
http://dx.doi.org/10.1017/CBO9780511535758.005
Cambridge Books Online © Cambridge University Press, 2016

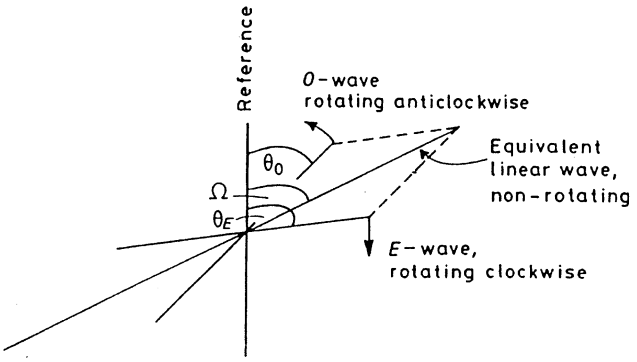

Figure 3.19. Addition of two circularly polarized waves to give a linear wave, as seen by a stationary observer looking along the geomagnetic field (from Hargreaves, 1992).

and

$$\theta_E = 2\pi f[t + n_E l/c], \tag{3.87}$$

giving

$$\Omega = (\pi f/c)(n_O - n_E)l. \tag{3.88}$$

At a sufficiently high frequency (e.g. >50 MHz) the gyrofrequency $f_B \ll f$, and then the ordinary and extraordinary refractive indices differ by

$$n_O - n_E = XY = (f_N^2 f_B)/f^3, \tag{3.89}$$

giving

$$\Omega = \frac{1}{2c}\frac{f_N^2 f_B}{f^2} l. \tag{3.90}$$

Therefore the polarization angle changes progressively as the wave travels through the ionized medium. On substituting values and allowing for varying electron density and magnetic field strength, we obtain

$$\Omega = \frac{8.448 \times 10^{-7}}{f^2}\int f_L N \mathrm{d}l$$
$$= \frac{2.365 \times 10^4}{f^2}\int B_L N \mathrm{d}l, \tag{3.91}$$

since $f_L = 2.799 \times 10^{10} B_L$, B_L being in webers m^{-2}. We have now moved to the QL approximation, to allow for propagation somewhat across the field. (In fact the QL approximation has wide application in the Faraday effect, being valid to a few degrees of normal to the field). As seen by an observer at the ground looking up, the polarization rotates anticlockwise in the northern hemisphere and clockwise

Downloaded from Cambridge Books Online by IP 141.211.4.224 on Wed Mar 23 15:38:40 GMT 2016.
http://dx.doi.org/10.1017/CBO9780511535758.005
Cambridge Books Online © Cambridge University Press, 2016

in the southern hemisphere, irrespective of the direction in which the wave is traveling. A recent extensive discussion of the Faraday effect is given by Yeh *et al.* (1999).

Absorption

Equation (3.61) gives the absorption coefficient κ in the case of non-deviative absorption and the QL approximation. The signal amplitude falls by a factor of e over the distance $1/\kappa$. Provided that the radio frequency is considerably greater than the critical frequency of the layer, this formula applies to trans-ionospheric propagation through the whole of the ionosphere. Whereas κ is in units of nepers, it is usual to express signal loss in decibels (dB), defined by the ratio between initial (P_1) and final (P_2) powers:

$$\text{Absorption } A\ (\text{dB}) = 10\log_{10}(P_1/P_2). \tag{3.92}$$

The neper and the decibel are related by

$$1\ \text{neper} = 8.686\ \text{dB}. \tag{3.93}$$

On putting in the appropriate values, Equation (3.92) gives

$$A\ (\text{dB}) = 4.611 \times 10^{-5} \int \frac{N\nu}{\nu^2 + (\omega \pm \omega_\text{L})^2}\,\text{d}l \tag{3.94}$$

for the total absorption over the path.

Since the collision frequency decreases sharply with altitude, most non-deviative absorption occurs in the lower ionosphere, and it is maximized when the terms in the denominator of Equation (3.94) are equal. If ν is the larger term, the absorption varies as $1/\nu$ and therefore decreases at the lower levels. However, over most of the height range affected the second term dominates and then the total absorption is just proportional to the integral of $N\nu$. Moreover, the gyrofrequency may be neglected if it is much smaller than the radio frequency, which is certainly the case at frequencies greater than about 30 MHz. Then Equation (3.94) simplifies to

$$A\ (\text{dB}) = \frac{1.168 \times 10^{-18}}{[f\,(\text{MHz})]^2} \int N\nu\,\text{d}l \tag{3.95}$$

for the total absorption over the path.

The limit to high-latitude communications is often set by the ionospheric absorption, and measuring the absorption of the cosmic radio noise is a valuable technique in high-latitude studies.

Downloaded from Cambridge Books Online by IP 141.211.4.224 on Wed Mar 23 15:38:40 GMT 2016.
http://dx.doi.org/10.1017/CBO9780511535758.005
Cambridge Books Online © Cambridge University Press, 2016

3.4.5 Principles of radio scintillation

Introduction

The phenomenon of scintillation, which appears principally in trans-ionospheric signals, is caused by relative phase shifts in the propagating wavefront and by subsequent diffraction. The phase shifts are a direct result of spatial irregularity in the medium and specifically in the electron content, to which they are related by Equation (3.82). It should be noted that, other things being equal, the irregular component of the electron content varies not linearly with the path length (*slab thickness*), but with its square root.

According to Huygens' principle, each part of a wavefront may be regarded as a source of secondary wavelets, whose superposition builds up the wavefront at a point further along. In diffraction theory this principle is applied to determine how the amplitude and phase of a received signal are affected by passage through a region of irregularities. Diffraction theory applies to "small" irregularities, the criterion for which is that there are at least several of them within the distance of the first Fresnel zone (see below).

Diffraction by a thin screen of weak irregularities and the concept of the angular spectrum

The simplest case to treat is that of a thin, shallow, phase-changing screen. In this model the irregularities are assumed to lie in an infinitely thin layer, and to introduce small (<1 radian) phase perturbations along the wavefront of a wave passing through it, as in Figure 3.20

The incident wave is planar (the source being located at infinity), but the emerging wavefront is irregular. To obtain the field at a point P in the observing plane OO′, it is necessary to sum the contributions from each point of the emerging wavefront, EE′. Since EE′ is irregular in phase, the field at OO′ will also be irregular, and in general both the phase and the amplitude are affected.

Since the wavefield at the observing plane is made up from contributions from points all along the diffracting screen, it is clear that there is not necessarily a one-to-one relationship between the irregularities in the ionosphere and the wavefield at the ground. There are, nevertheless, some relationships of a statistical nature.

The link between the properties of the screen and the variations observed at the ground is the *angular spectrum* of the waves leaving the screen. Just as a wave modulated in time may be expressed as a frequency spectrum that may be derived by a Fourier transformation, so a wave modulated in distance may be expressed by a spectrum in angle. The spectrum of periodicities in the screen, $F(d)$, is related by Fourier transformation to an angular spectrum of waves, $f(\sin\theta)$, where d is the spatial wavelength of irregularities and θ is the angle of propagation measured from the normal. The same spectrum reaches the ground, though with the phase of each sine wave modified by the distance traveled, where it may be transformed back to a

Downloaded from Cambridge Books Online by IP 141.211.4.224 on Wed Mar 23 15:38:40 GMT 2016.
http://dx.doi.org/10.1017/CBO9780511535758.005
Cambridge Books Online © Cambridge University Press, 2016

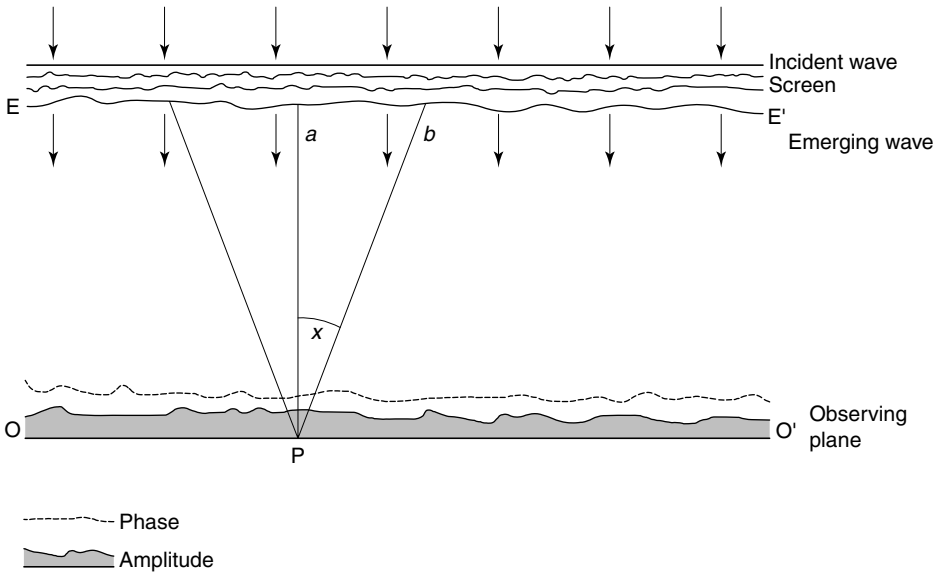

Figure 3.20. Diffraction of a plane wave incident on a thin phase-changing screen.

wavefield in the observing plane. Both F and f are complex, and therefore full information may be obtained only by observing both the amplitude and the phase.

The problem now is that, whereas it is easy to measure the amplitude of a received radio signal, it is much more difficult to measure the phase. However, it has been shown that, if the observations are made sufficiently far from the screen (and provided that the screen is shallow – i.e. the initial modulation is only small), the statistical properties of the amplitude and phase irregularities at the ground are the same as each other and the same as those at the screen. In that case, amplitude observations alone suffice to give the statistical properties of the ionospheric screen.

It is unlikely that irregularities will be sinusoidal or have any other analytical form; they will more probably look like random noise. Such irregularities may be handled using the correlation function, ρ.

If $a(x)$ are the differences of a varying quantity $A(x)$ from its mean $\bar{A}$, and σ^2 is the variance of $a = [A(x) - \bar{A}]^2$ (the bars denoting averages over many values), the correlation function of A over the interval y is

$$\rho(y) = [\overline{a(x)a(x+y)}]/\sigma^2. \tag{3.96}$$

The correlation function may sometimes be assumed to have a Gaussian form,

$$\rho(d) = \exp[-d^2/(2d_0^2)] \tag{3.97}$$

and in this case the angular power spectrum would also be Gaussian:

$$\mathrm{P}(\sin\theta) = \exp[-\sin^2\theta/(2\sin^2\theta_0)], \tag{3.98}$$

Downloaded from Cambridge Books Online by IP 141.211.4.224 on Wed Mar 23 15:38:40 GMT 2016.
http://dx.doi.org/10.1017/CBO9780511535758.005
Cambridge Books Online © Cambridge University Press, 2016

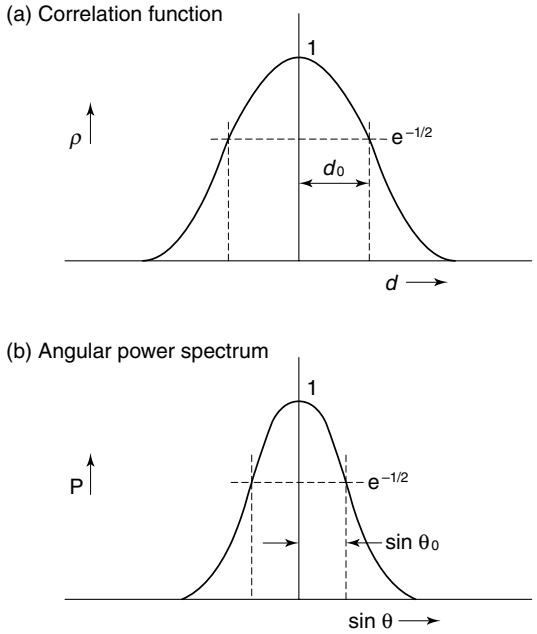

Figure 3.21. (a) Correlation function and (b) angular power spectrum for a random diffraction screen.

where

$$\sin\theta_0 = \lambda/(2\pi d_0). \tag{3.99}$$

Figure 3.21 illustrates the relationship between ρ and P in this case.

Fresnel-zone effects

The distance between the screen and the observer is significant because the size of the Fresnel zones depends upon the distance as well as the wavelength. Recall that, by definition, the first Fresnel zone extends to the point where the distance to the observer exceeds the minimum distance by $\lambda/2$, the resulting phase difference being 180°. Referring to Figure 3.20, if the overhead point is a, we can pick a point b such that $P_b - P_a = \lambda/4$. If the screen alters the phase only, the signal at EE′ may be sketched as in Figure 3.22(a), where A is the unaffected signal and α_E is the perturbation due to the screen.

At a point P on the observing plane, if the perturbation due to a alters the phase of the signal, that due to b will affect its amplitude because of the extra $\lambda/4$ traveled. The resulting signal might now look like Figure 3.22(b), with both phase and amplitude fluctuations involved.

Since contributions may affect the amplitude only if they fall within the angular spectrum, it follows that

$$(\lambda D/2)^{1/2} > \pi d_0 \tag{3.100}$$

Downloaded from Cambridge Books Online by IP 141.211.4.224 on Wed Mar 23 15:38:40 GMT 2016.
http://dx.doi.org/10.1017/CBO9780511535758.005
Cambridge Books Online © Cambridge University Press, 2016

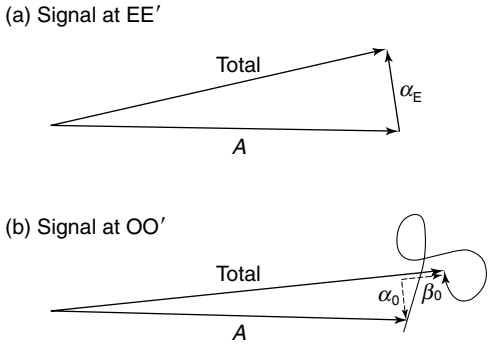

Figure 3.22. Development of (a) phase and (b) amplitude perturbations from initial perturbations.

for amplitude scintillation to appear at an observing plane at distance D from a pure phase screen, the source being at infinity. This says that the signal received from a phase screen will contain both amplitude and phase perturbations if the observer is sufficiently far from the screen for the first Fresnel zone to contain several irregularities of typical size. At infinity, the fading power becomes equally divided:

$$\begin{aligned}\sigma(A)/\bar{A} &= \sigma(\phi) \\ &= \sigma_s(\phi)/\sqrt{2},\end{aligned} \tag{3.101}$$

where $\sigma(A)$ and $\sigma(\phi)$ are the standard deviations of amplitude and phase.

At a lesser distance there will be phase fluctuation, but the amplitude fluctuation will not be fully developed, and this is often the situation in practice. If the radio wavelength, λ, is 6 m and the irregular screen is 400 km away, the radius of the first Fresnel zone is $\sqrt{\lambda D} = 1.5$ km. Many of the irregularities will be larger than that and therefore the amplitude fluctuations will not be fully developed.

The properties of a phase screen are important because the ionosphere behaves as a phase screen in most cases, and the bulk motion of the irregularities causes the signal received at a fixed place to scintillate. If, by means of a specially devised experiment, it is possible to observe phase as well as amplitude scintillation, the Fresnel-zone effect can be investigated directly by comparing the spectra of phase and amplitude fluctuations. An example is shown in Figure 3.23

The irregularities in the ionosphere generally exhibit a power-law spectrum of form κ^{-P}, where κ is the wave number ($2\pi/d$, in which d is the spatial wavelength of the irregularities). We may generally suppose that the phase screen in the ionosphere produces a pattern of amplitude and phase fluctuation over the ground that is related to the spectrum of the irregularities themselves, and that scintillations are observed because the pattern is moving across the observing point. It is by this means that the variation in distance is converted into a time variation. Since the conversion of phase to amplitude scintillation depends on the size of the irregularity, the low-frequency (arising from the large scale) end of the spectrum

Downloaded from Cambridge Books Online by IP 141.211.4.224 on Wed Mar 23 15:38:40 GMT 2016.
http://dx.doi.org/10.1017/CBO9780511535758.005
Cambridge Books Online © Cambridge University Press, 2016

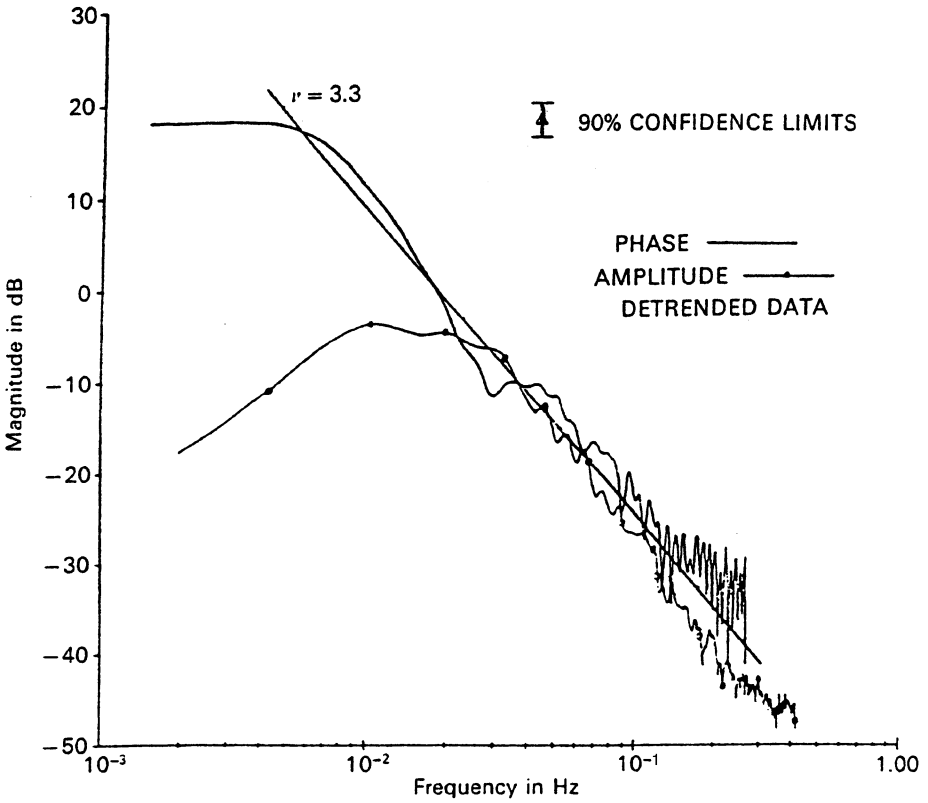

Figure 3.23. Spectra of the amplitude and phase recorded at 40 MHz from a geosynchronous satellite transmission. Power spectra are plotted on a log scale of relative values in decibels. The phase spectrum levels off due to detrending (at 3×10^{-3} Hz), but the turn in the amplitude spectrum marks the Fresnel frequency. (After W. J. Myers *et al.*, *J. Geophys. Res.* **84**, 2039 (1979), copyright by the American Geophysical Union.)

is attenuated. The attenuation operates at frequencies less than $u/\sqrt{2\lambda D}$, where u is the velocity (it being assumed that all the irregularities move together) and $\sqrt{\lambda D}$ is the radius of the first Fresnel zone. Since λ is known and D may be assumed (to be approximately 350 km), u can be determined by this means. This effect is seen in the spectra of Figure 3.23. When spectra can be determined, one can therefore obtain further information about the irregularities and their motion, particularly if the "Fresnel frequency" can be identified.

The above results are altered if the source is not at infinity (because the wavefront reaching the screen is then curved), and/or the phase screen introduces deep modulation, $\sigma_s(\phi) > 1$ radian (since that broadens the angular spectrum).

There is an extensive body of literature on the theory of scintillations. Hargreaves (1992) gives further details at an introductory level. The basic theory and early work were reviewed by Ratcliffe (1956), and later developments by Yeh and Liu (1982).

Downloaded from Cambridge Books Online by IP 141.211.4.224 on Wed Mar 23 15:38:40 GMT 2016.
http://dx.doi.org/10.1017/CBO9780511535758.005
Cambridge Books Online © Cambridge University Press, 2016

Indices and simple statistics of scintillation

The intensity of amplitude scintillation is usually expressed by using one of four indices (Briggs and Parkin, 1963). If A is the amplitude, $\bar{A}$ is the mean amplitude, P is the power, $P = A^2$, $\bar{P}$ is the mean power, $a = A - \bar{A}$, and $p = P - \bar{P}$,

$$S_1 = |\bar{a}|/\bar{A}, \tag{3.102}$$

$$S_2 = (\overline{a^2})^{1/2}/\bar{A}, \tag{3.103}$$

$$S_3 = |\bar{p}|/\bar{P}, \tag{3.104}$$

$$S_4 = (\overline{p^2})^{1/2}/\bar{P}. \tag{3.105}$$

These are all dimensionless. S_1 is the mean deviation of the amplitude normalized by the mean amplitude, and S_2 the root-mean-square deviation of the amplitude also divided by the mean amplitude. S_3 is the mean deviation of the power normalized by the mean power, and S_4 the root-mean-square deviation of the power, similarly normalized. Note that S_3 and S_4 are similar to S_1 and S_2 but are written in terms of power instead of amplitude. From this selection of indices, S_4 is the most commonly used.

It has been shown (Chytil, 1967) that the following approximate relations apply:

$$\begin{aligned} S_1 &= 0.42 S_4, \\ S_2 &= 0.52 S_4, \\ S_3 &= 0.78 S_4. \end{aligned} \tag{3.106}$$

An example of weak scintillation is shown in the top three panels of Figure 3.24.

The S_4 values are 0.016, 0.076, and 0.54 at 360, 140, and 40 MHz, respectively, all of which are less than unity. The bottom panel of Figure 3.24 gives the amplitude spectra, normalized with respect to magnitude for easier comparison. The turnover points indicate Fresnel frequencies of 0.07, 0.045, and 0.025 Hz, respectively, varying approximately as the square root of the radio frequency. The fading spectrum varies as (fading frequency)$^{-3.5}$. For comparison, Figure 3.25 illustrates the appearance of records with deep scintillation. Here the S_4 values are respectively 0.13, 0.54, and 1.42. The character of the record changes dramatically when the modulation becomes deep.

In Figure 3.22b, the fading signal is represented as a steady component plus random in-phase and quadrature components. If the random components are small relative to the steady one, the amplitude of the total signal (A) will fluctuate about the mean with a Gaussian distribution. At the other extreme, if the steady component is small relative to the random one, the amplitude distribution will be a "random walk" having the Rayleigh form. Between these extremes the family of *Nakagami m-distributions* (Nakagami, 1960) applies. Figure 3.26 illustrates

Downloaded from Cambridge Books Online by IP 141.211.4.224 on Wed Mar 23 15:38:40 GMT 2016.
http://dx.doi.org/10.1017/CBO9780511535758.005
Cambridge Books Online © Cambridge University Press, 2016

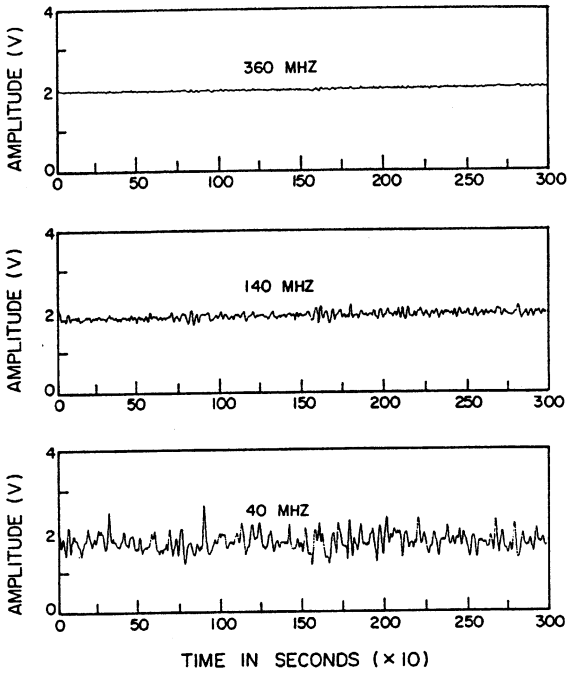

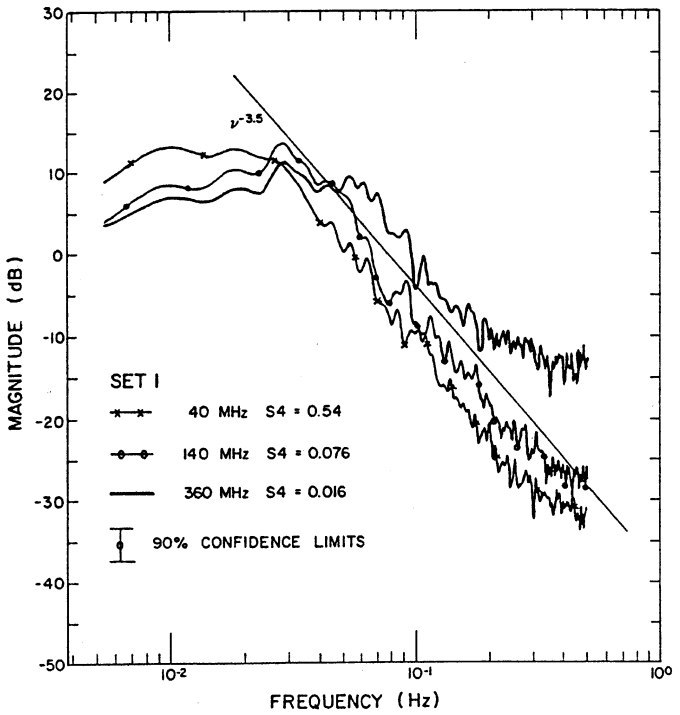

Figure 3.24. Examples of amplitude scintillation at three frequencies from a geosynchronous satellite, and their spectra. (R. Umeki *et al.*, *J. Geophys. Res.*, **82**, 2752 (1997b).)

Downloaded from Cambridge Books Online by IP 141.211.4.224 on Wed Mar 23 15:38:40 GMT 2016.
http://dx.doi.org/10.1017/CBO9780511535758.005
Cambridge Books Online © Cambridge University Press, 2016

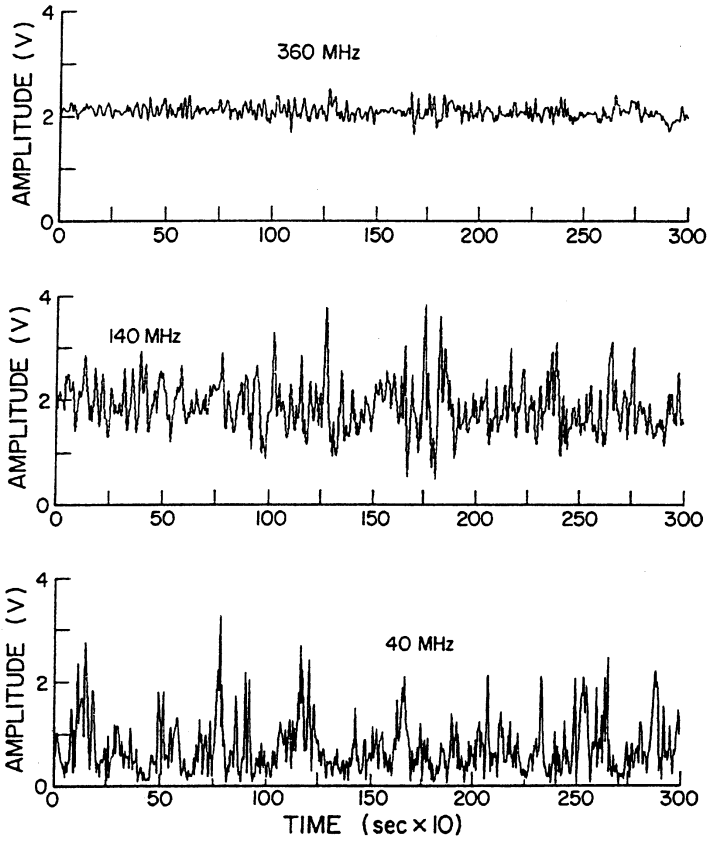

Figure 3.25. Scintillations at 360, 140, and 40 MHz, showing the transition to deep fading: $S_4 = 0.13$, 0.54, and 1.42. (R. Umeki *et al.*, *Radio Science*, **12**, 311 (1997a).)

amplitude distributions for various S_4 values covering the range between the Gaussian ($S_4 = 0.1$) and the Rayleigh.

Figure 3.27 gives a range of phase distributions, all of which are, of course, symmetrical about zero, The m-distributions are characterized by a single parameter that can be related to S_4 and to the standard deviation of the phase.

3.4.6 Propagation involving reflection from a sharp boundary and full-wave solutions

Reflection at a boundary

The treatment of propagation outlined in the foregoing sections, which are based on the concept of the refractive index, assumes that the medium is uniform. Of course this is seldom the case, but in practice the assumption may be used provided that any variations are not too large over a distance of several wavelengths. Such a medium is said to be *slowly varying.* There are, however, situations in which

Downloaded from Cambridge Books Online by IP 141.211.4.224 on Wed Mar 23 15:38:40 GMT 2016.
http://dx.doi.org/10.1017/CBO9780511535758.005
Cambridge Books Online © Cambridge University Press, 2016

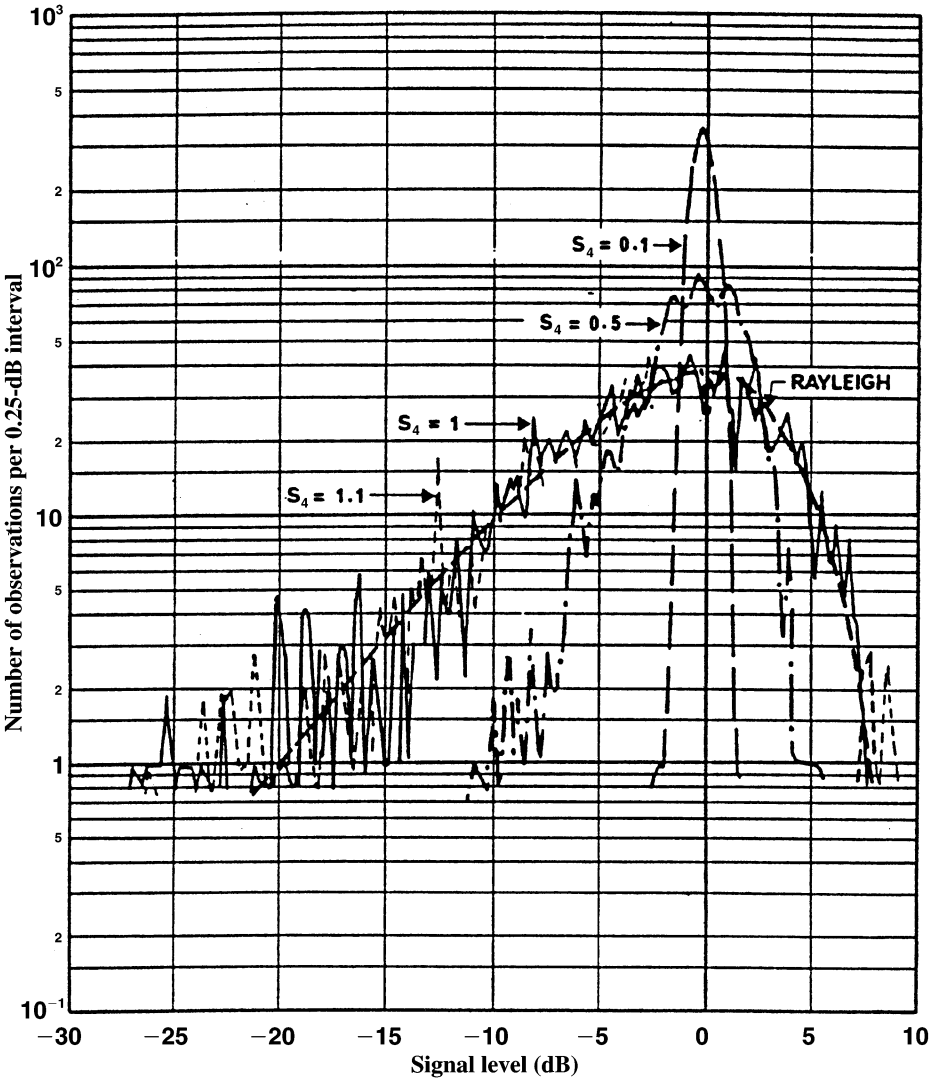

Figure 3.26. Empirical amplitude distributions for a range of S_4 values. (After R. K. Crane, Technical Note 1974–26, Lincoln Laboratory (1974).)

this is plainly not so, and then a different sort of treatment is required.

If the medium changes significantly within a wavelength then we may use the physics of reflection at a sharp boundary, as at a partially reflecting mirror. If a wave is normally incident at a sharp boundary, the coefficients of reflection and transmission are determined by the condition that the tangential components of the **E** and **H** vectors must be continuous across the boundary

Referring to Figure 3.28, where the subscripts i, t, and r mean incident, transmitted, and reflected, the wave being incident from below,

$$E_t = E_I + E_r \tag{3.107}$$

Downloaded from Cambridge Books Online by IP 141.211.4.224 on Wed Mar 23 15:38:40 GMT 2016.
http://dx.doi.org/10.1017/CBO9780511535758.005
Cambridge Books Online © Cambridge University Press, 2016

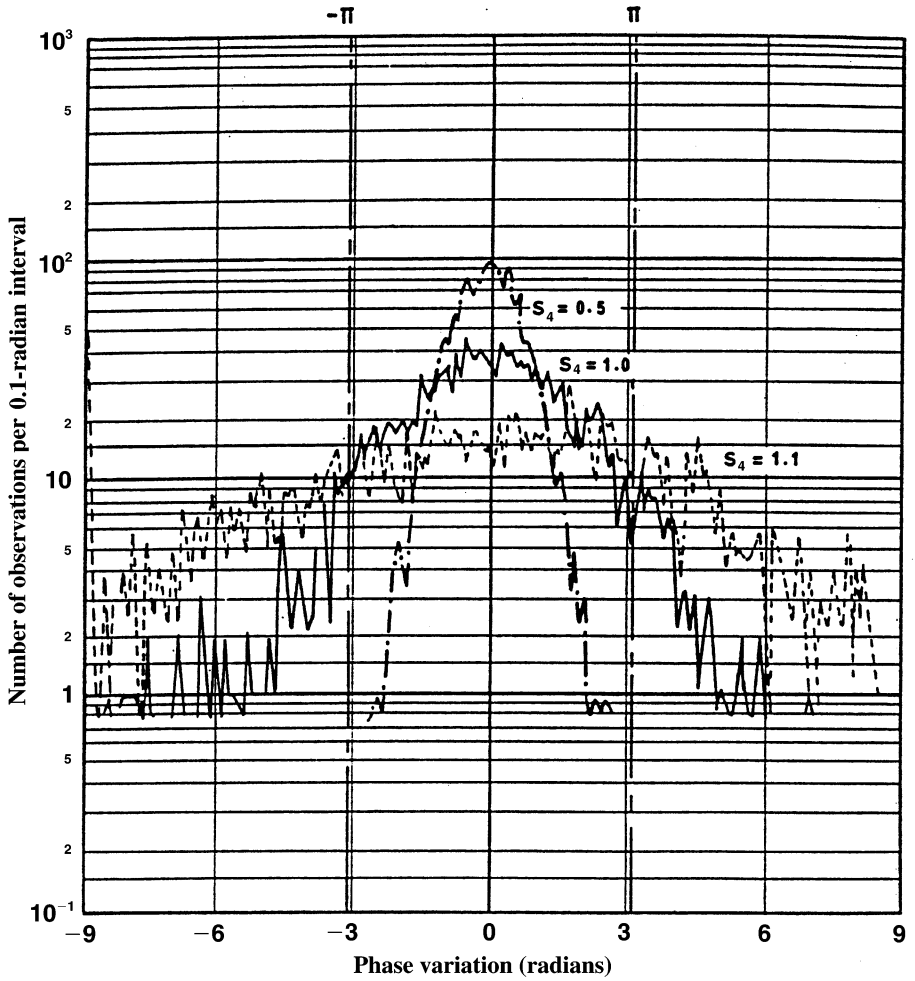

Figure 3.27. Empirical phase distributions for a range of S_4 values. (After R. K. Crane, Technical Note 1974–26, Lincoln Laboratory (1974).)

and

$$H_t = H_i - H_r, \tag{3.108}$$

the negative sign arising because the reflected wave propagates downward. In a non-magnetic medium,

$$H/E = n/(\varepsilon_0 \mu_0)^{1/2} \tag{3.109}$$

and, by substitution, the reflection coefficient ρ is given by

$$\rho = E_r/E_I = (n_2 - n_1)/(n_2 + n_1). \tag{3.110}$$

The fraction of power reflected is $(E_r/E_i)^2$.

Downloaded from Cambridge Books Online by IP 141.211.4.224 on Wed Mar 23 15:38:40 GMT 2016.
http://dx.doi.org/10.1017/CBO9780511535758.005
Cambridge Books Online © Cambridge University Press, 2016

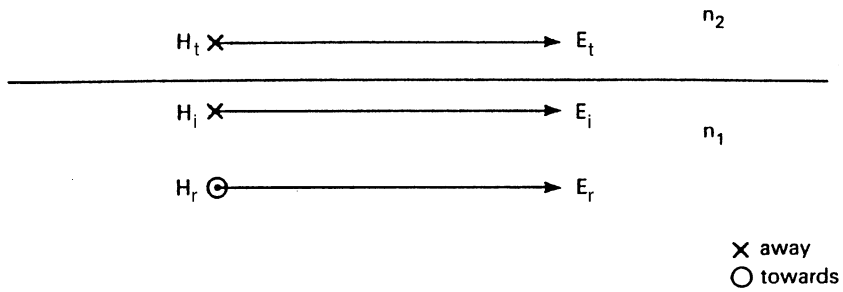

Figure 3.28. The continuity of electric and magnetic vectors at a sharp boundary.

When the wave is incident at an angle to the boundary a further condition must be applied, which is that the normal components of the electric and magnetic flux (εE and μH) are also continuous across the interface. One familiar result that follows is *Snell's Law*:

$$n_1 \sin\theta_I = n_2 \sin\theta_t, \tag{3.111}$$

where θ_i is the angle of incidence in the medium of refractive index n_1, and θ_t is the angle of the ray transmitted into medium n_2.

We now consider two special cases. First, let the plane of polarization (by convention the direction of the electric field) be perpendicular to the plane of incidence. Then application of the continuity conditions gives

$$\rho_\perp = \sin(\theta_i - \theta_t)/\sin(\theta_i + \theta_t), \tag{3.112}$$

or,

$$\rho_\perp = \frac{\sqrt{(n_2/n_1)^2 - \sin^2\theta_i} - \cos\theta_i}{\sqrt{(n_2/n_1)^2 - \sin^2\theta_i} + \cos\theta_i}. \tag{3.113}$$

This is the *first Fresnel equation* for reflection.

If the plane of polarization lies in the plane of incidence, the reflection coefficient is given by

$$\rho_\parallel = \tan(\theta_i - \theta_t)/\tan(\theta_i + \theta_t) \tag{3.114}$$

$$= \frac{(n_2/n_1)^2\cos\theta_i - \sqrt{(n_2/n_1)^2 - \sin^2\theta_i}}{(n_2/n_1)^2\cos\theta_i + \sqrt{(n_2/n_1)^2 - \sin^2\theta_i}}. \tag{3.115}$$

This is the *second Fresnel equation.* When $\theta_i + \theta_t = 90°$, $\tan(\theta_i + \theta_t) = \infty$, and then $\rho_\parallel = 0$. This is the *Brewster angle*, given by $\tan\theta_B = n_2/n_1$, where the reflection coefficient goes to zero if the **E** vector is in the plane of incidence – in practice, the wave is vertically polarized. The reflected wave is reversed in phase as the Brewster angle is crossed. There is no such effect if the wave is horizontally polarized.

Downloaded from Cambridge Books Online by IP 141.211.4.224 on Wed Mar 23 15:38:40 GMT 2016.
http://dx.doi.org/10.1017/CBO9780511535758.005
Cambridge Books Online © Cambridge University Press, 2016

At normal incidence Equations (3.113) and (3.115) both revert to (3.110). At grazing incidence, as $\theta_i \to 90°$, $\rho_\parallel \to 1$, but $\rho_\perp \to -1$, implying that there is a reversal of phase on reflection.

These remarks apply to reflection at the interface between dielectrics, n_1 and n_2 being both real. If the reflector is a partial conductor, the Fresnel equations still apply but the refractive indices are now complex. In the general case reflection involves a change of phase as well as of amplitude. Provided that the conditions of a sharp boundary are satisfied and the appropriate refractive indices are used, the Fresnel formulae are of wide application throughout the electromagnetic spectrum.

Full-wave solutions

There are (unfortunately) other cases in which the medium changes over a radio wavelength but the change is not sharp enough to count as a sharp boundary. In these cases the only approach is to develop a *full-wave solution*, which amounts to solving Maxwell's equations at each step through the layer by a numerical method. Conditions are imposed above and below the spatially varying medium to correspond to incident waves, and then the transmitted and reflected waves may be deduced. Though the method is applicable generally, preference would obviously be given to the simpler ones where they are valid. For more information about this technique the reader is referred to Budden (1985).

Sub-ionospheric propagation at ELF and VLF

At frequencies below about 30 kHz the base of the ionosphere is only a few wavelengths above the ground, and across the boundary the ionosphere alters greatly within a wavelength. The propagation may now be considered in terms of reflection at a sharp boundary. At oblique incidence the loss on reflection is relatively small, and in consequence these signals may propagate over great distances with an attenuation amounting to only 2–3 dB per 1000 km. They exhibit some interesting properties, one being that (except at high latitude) the diurnal variation is more predictable than it is at higher frequencies, which makes them particularly suitable for those applications, such as navigation and time transmission, which require high stability.

In the lower ionosphere the collision frequency (2×10^6 s^{-1} at 70 km height) is greater than the wave frequency at VLF. Neglecting the magnetic field, Equation (3.55) then gives the refractive index (n) as

$$n^2 = |1 - \mathrm{j}X/2| = 1 - \omega_N^2/(\mathrm{j}\omega\nu). \tag{3.116}$$

The ionosphere now behaves as a metal rather than a dielectric, having conductivity

$$\sigma = (\varepsilon_0 \omega_N^2)/\nu = Ne^2/(m_e \nu), \tag{3.117}$$

where ν is the collision frequency.

Downloaded from Cambridge Books Online by IP 141.211.4.224 on Wed Mar 23 15:38:40 GMT 2016.
http://dx.doi.org/10.1017/CBO9780511535758.005
Cambridge Books Online © Cambridge University Press, 2016

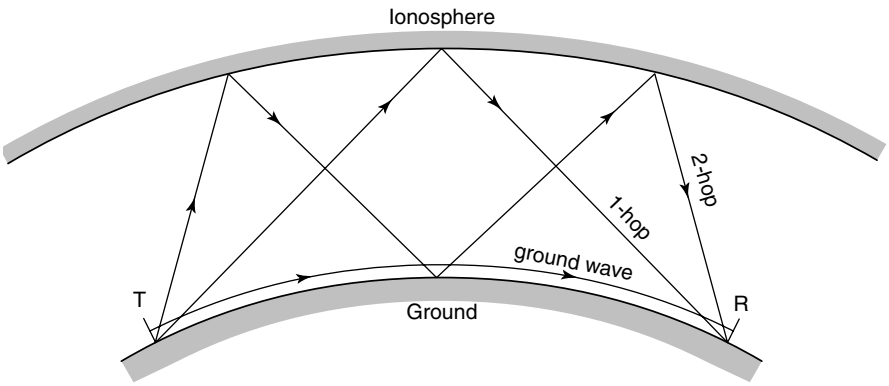

Figure 3.29. Propagation in terms of a ground wave and two skywaves.

Studies of the amplitude and phase of VLF signals received from transmitters at various distances indicate the effective reflection height (about 70 km by day) and the ionospheric conductivity. Reflection coefficients are typically 0.2–0.5 There are actually four reflection coefficients because the presence of the geomagnetic field causes changes of polarization on reflection as well as of amplitude and phase.

Putting typical values into the criterion of Equation (3.31) confirms that, at VLF and ELF, the lower ionosphere behaves as a conductor. Then, inserting the condition $[\sigma/(\omega\varepsilon)]^2 \gg 1$ into Equation (3.29) leads to a skin depth (at which the amplitude falls by a factor of 1/e) of

$$1/\alpha = \sqrt{\varepsilon_0 \lambda c/(\pi\sigma)}. \tag{3.118}$$

The skin depth varies as the square root of the wavelength and inversely as the square root of the conductivity. The ground is also a partial conductor, and, even in sea water, the most highly conducting part of the Earth's surface, there is sufficient penetration to permit VLF and ELF communication with submerged submarines.

Over distances up to several hundred kilometers, VLF propagation can be treated by summing the ground wave and the first few hops (Figure 3.29). This is the basis of *geometrical-optical*, or *ray*, theory.

For long-distance propagation, one must resort to waveguide theory as developed by Budden (1961) and Wait (1970) and illustrated in Figures 3.30 and 3.31. This waveguide treatment is applicable because both the Earth and the ionosphere are partial conductors separated by a few wavelengths. In Figure 3.30 one assumes that the signal at a point consists of component wavelets emanating from images of the source.

For long-distance VLF propagation the ionosphere behaves approximately like a conductor with a reflection coefficient of -1 and the ground has a reflection coefficient of $+1$. As in Figure 3.30, the *images* are located at $z = \pm 2h, \pm 4h, \ldots,$

Downloaded from Cambridge Books Online by IP 141.211.4.224 on Wed Mar 23 15:38:40 GMT 2016.
http://dx.doi.org/10.1017/CBO9780511535758.005
Cambridge Books Online © Cambridge University Press, 2016

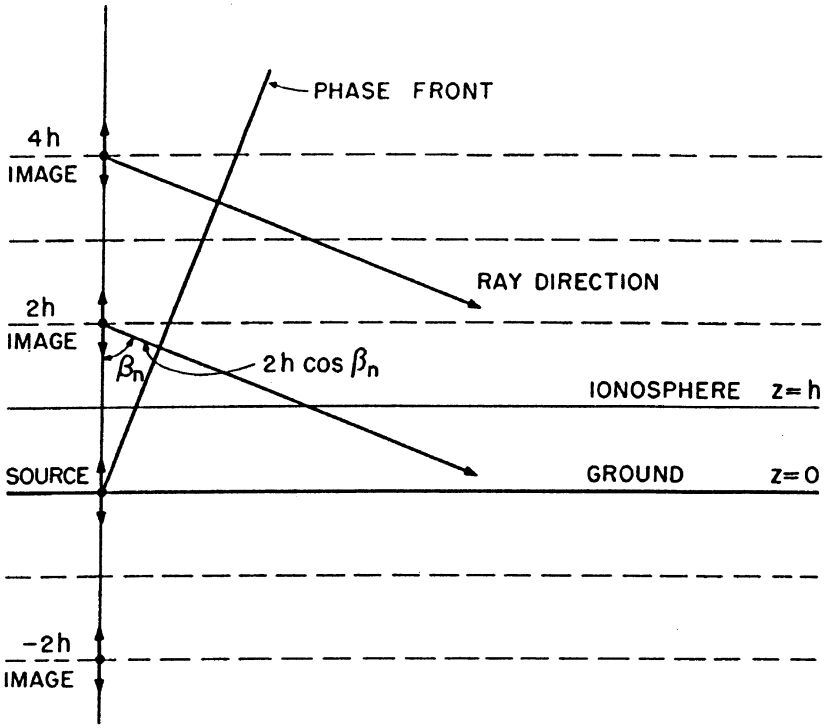

Figure 3.30. Using the method of images to construct one of the pair of waves that will interfere to produce the field patterns in the waveguide, such as those shown in Figure 3.31. The second wave (not shown) comes from the negative side. (After Davies, 1990.)

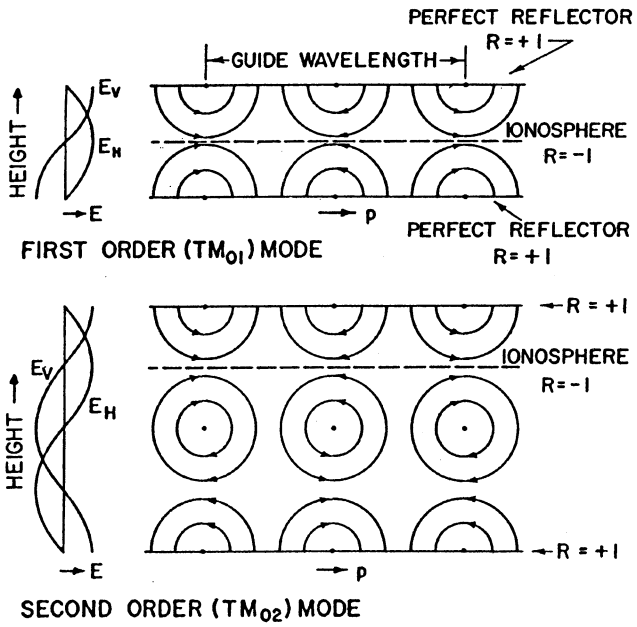

Figure 3.31. An idealization of the **E** field in the Earth–ionosphere waveguide for waves polarized with their electric fields in the vertical plane and their magnetic fields transverse to the plane of propagation (TM_{02} mode) (from Davies, 1990).

Downloaded from Cambridge Books Online by IP 141.211.4.224 on Wed Mar 23 15:38:40 GMT 2016.
http://dx.doi.org/10.1017/CBO9780511535758.005
Cambridge Books Online © Cambridge University Press, 2016

but now they alternate in sign, which is equivalent to a change in phase of π, and resonance occurs at

$$2hC_n = \left(n - \tfrac{1}{2}\right)\pi, \tag{3.119}$$

where C_n is $n\lambda/(2h)$ and $n = +1, +2, \ldots$.

In Figures 3.30 and 3.31 there is no zeroth-order mode and the horizontal wavelength $\lambda_g = \lambda/S_n$ is given by

$$(1/\lambda_g)^2 = (1/\lambda)^2 - [n/(2h)]^2, \tag{3.120}$$

where S_n is the Fresnel coefficient showing that, for $\lambda > 2h/n$, λ_g is imaginary and hence the mode is evanescent. Thus there is a minimum cutoff frequency, f_n, below which waves will not propagate, where $f_n = nc/(2h)$.

The cutoff frequency for the first-order mode during daytime, when the height of the ionospheric D region is low, $\approx$2 kHz. For the case of a conducting ionosphere, the cutoff frequency is given by

$$f_n = \left(n - \tfrac{1}{2}\right)c/(2h). \tag{3.121}$$

So we see that the change of reflection coefficient R from $+1$ to -1 changes the cutoff frequency (for $n = 1$) from about 2 Hz to 1 kHz. When they are being compared with waveguide modes with perfectly conducting walls, the ideal Earth–ionosphere modes should be denoted by $n - \frac{1}{2}$, rather than by n. A more complete analysis of the VLF waveguide mode must include Earth–ionosphere irregularities, changes in the height of the ionosphere, the effect of the geomagnetic field and collisions of electrons. There is a voluminous literature on VLF propagation (see Budden, 1985, references; and Davies, 1990, pp. 371–379).

The main *natural* sources at ELF are lightning discharges, and the actual use of ELF for propagating signals is quite limited because of the practical constraints on constructing antennas several thousand meters long. Another important feature of ELF propagation is that the distance between source and receiver may be comparable to the wavelength (for example, a 300-Hz ELF signal has a wavelength of $\lambda = 1000$ km. At these extremely low frequencies, the ionosphere behaves more like a conductor than a conducting dielectric and the displacement current is small. Because of this large *skin depth* (see Ramo *et al.* 1965, pp. 249–299) in the D region for ELF, the reflection height is $\approx$90 km.

As an actual example, the U. S. Navy's Wisconsin Test Facility (WTF) radiates frequencies in the 40–50 and 70–80 Hz ranges. At the WTF the antennas are two 22.5-km quasi-orthogonal antennas. At middle latitudes the attenuation rate at 75 Hz is about 1.2 dB Mm^{-1} during the day and 0.8 dB Mm^{-1} at night. ELF propagation is discussed in considerable detail in the June 1974 Proceedings of the IEEE. Anomalously strong ELF signals have also been received at *antipodal* regions (Fraser-Smith and Bannister, 1997).

Downloaded from Cambridge Books Online by IP 141.211.4.224 on Wed Mar 23 15:38:40 GMT 2016.
http://dx.doi.org/10.1017/CBO9780511535758.005
Cambridge Books Online © Cambridge University Press, 2016

Partial reflections at MF and HF

Turbulence in the lower ionosphere, at heights up to about 100 km, produces spatial irregularities on a scale sufficiently fine that partial reflections may be detected from them in the band 2–6 MHz (wavelengths 1.5 km to 500 m). In this case the reflections are very weak, a mere 10^{-3} to 10^{-5} of the amplitude of a total reflection, but they may be observed using a transmitter of high power and a large antenna array for transmission and reception. Although they are not useful for communications, these partial reflections may be exploited in a technique for measuring the electron-density profile of the lower ionosphere.

3.4.7 Whistlers

Whistlers are bursts of electromagnetic radiation in the VLF range that are produced by lightning discharges. These bursts travel through the ionosphere and magnetosphere in ducts approximately parallel to lines of force in the geomagnetic field and can be detected using low noise amplifiers with short antennas. Since about 1951 these signals have been studied scientifically for the information they reveal about the ionospheric and magnetospheric plasma. Other natural VLF emissions (called dawn chorus, risers, hiss, etc.) which are thought to originate in the ionosphere can also be heard on whistler detection equipment. Some of the fascination with the whistler phenomenon is due to the fact that it is a remarkable sound in the audio range, resembling a human whistle, that can be heard on sensitive audio equipment and on telephone lines under certain circumstances. The history of the scientific study of whistlers is covered by Eckersley (1925, 1928, 1929, 1931, and 1932), Helliwell (1965, 1988), Davies (1990), Hunsucker (1991), and in reviews by Park and Carpenter (1978) and Carpenter (1988).

The starting points for whistler theory are Appleton's equations for dispersion and polarization and the QL approximation. Figure 3.32 is a simplified presentation of basic whistler signatures obtained near the source and near the conjugate area of the source (i.e. the other end of the field line).

Another basic feature (not always present on a signature) is the "nose" (Helliwell, 1965) illustrated in Figure 3.33.

Helliwell (1965) showed that energy flow in the whistler will be guided along ducts in the geophysical magnetoplasma according to the following relation:

$$\tan(\theta-\alpha)\approx(0.5\tan\theta)/\left(1+\tfrac{1}{2}\tan^2\theta\right), \tag{3.122}$$

where α is the angle between the ray path of the whistler and the wave normal, θ is the propagation angle limited by $0<\theta<\theta_{\max}$, and $f_H\cos\theta_{\max}=f$, where f_H is the electron gyrofrequency.

Another important characteristic of a whistler wave packet is that the group velocity, v_g, is

$$v_g=2c[f^{1/2}(|f_L|-f)]/|f_L|f_N \tag{3.123}$$

Downloaded from Cambridge Books Online by IP 141.211.4.224 on Wed Mar 23 15:38:40 GMT 2016.
http://dx.doi.org/10.1017/CBO9780511535758.005
Cambridge Books Online © Cambridge University Press, 2016

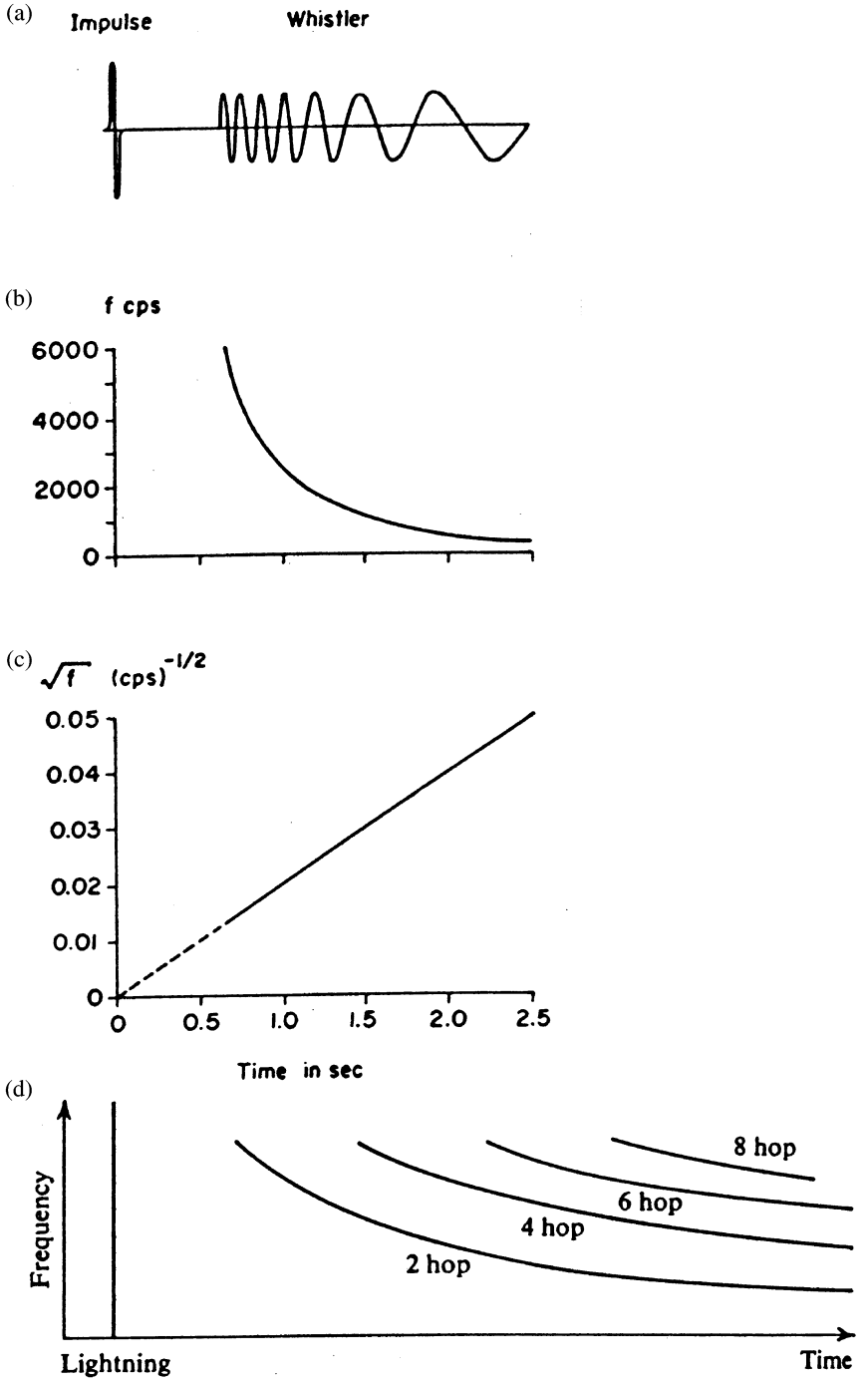

Figure 3.32. A sketch of the basic manifestation of a whistler and its initiating disturbances: (a) illustrating the dispersion; (b) the frequency–time curve of a typical whistler; (c) the curve of $\sqrt{f}$ with time, and (d) the initiating disturbance and multiple hops when the source and receiver are at the same end of a geomagnetic field-line (from Helliwell, 1965).

Downloaded from Cambridge Books Online by IP 141.211.4.224 on Wed Mar 23 15:38:40 GMT 2016.
http://dx.doi.org/10.1017/CBO9780511535758.005
Cambridge Books Online © Cambridge University Press, 2016

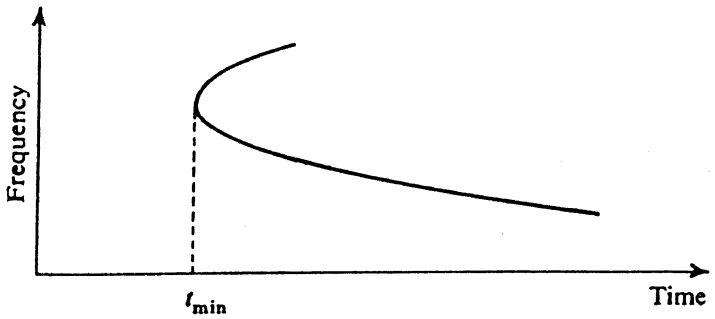

Figure 3.33. An idealized sketch of the frequency-versus-time characteristics of a "nose whistler" (from Helliwell, 1965).

where f_L is the longitudinal component of f_B and $f_L \gg f$, Equation (3.123) simplifies to

$$v_g = 2c(f^{1/2} f_L^{1/2})/f_N. \tag{3.124}$$

The dispersion law for whistlers is

$$T = \frac{1}{2c} \int_s f_N f_L \, ds/[f^{1/2}(f_L - f)^{3/2}], \tag{3.125}$$

which can be applied to determine $\int N \, dl$ along the field line.

3.5 Ionospheric scatter

One can qualitatively describe ionospheric scattering as either *strong* or *weak* in terms of the received signal strength of the scattered wave at the receiving radar antenna. An example of the former is VHF/UHF backscatter echoes received from electron density gradients in the auroral or equatorial ionosphere, and an example of the latter is incoherent backscatter by a VHF/UHF radar from the undisturbed E or F layer.

Another way of classifying scattered echoes is in terms of their *backscatter cross-section* (σ, in m^2) using pulsed radar systems, and their *temporal stability.* A *coherent echo* exhibits a statistical correlation of the amplitude and phase from one pulse to another, and emanates from quasi-deterministic gradients in electron density that have correlation times greater than 1 ms, which corresponds to a spectral width of the radar echo of less than 1000 Hz (sometimes less than 100 Hz). It also has a backscatter cross-section 10^4–10^9 times greater than that from an incoherent-scatter radar echo.

3.5.1 Coherent scatter

Other important considerations in the case of *coherent* backscatter are the relation between the *size* of the scattering irregularity relative to the free-space wavelength

Downloaded from Cambridge Books Online by IP 141.211.4.224 on Wed Mar 23 15:38:40 GMT 2016.
http://dx.doi.org/10.1017/CBO9780511535758.005
Cambridge Books Online © Cambridge University Press, 2016

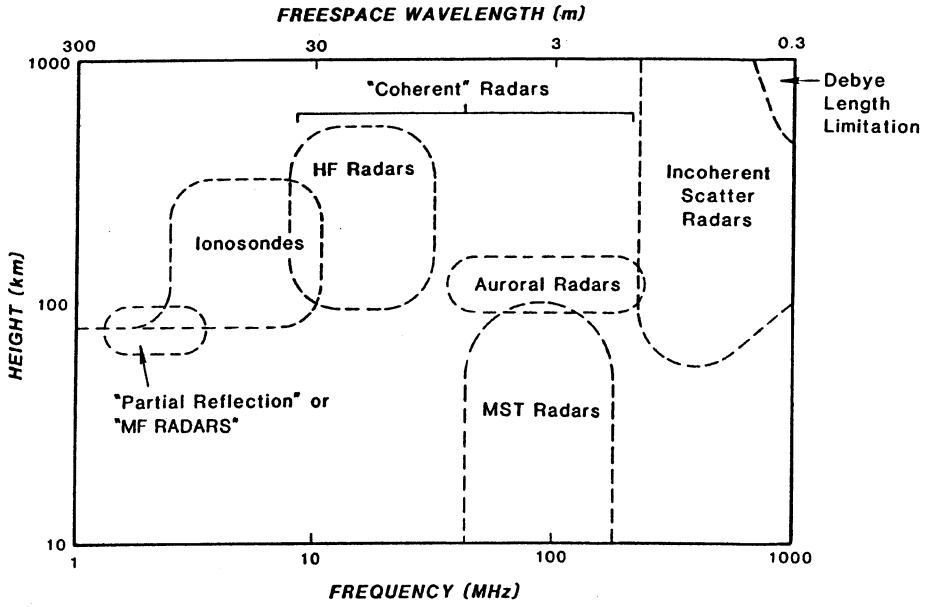

Figure 3.34. Height–frequency regimes of various ionospheric radar probes (from Schlegel, 1984).

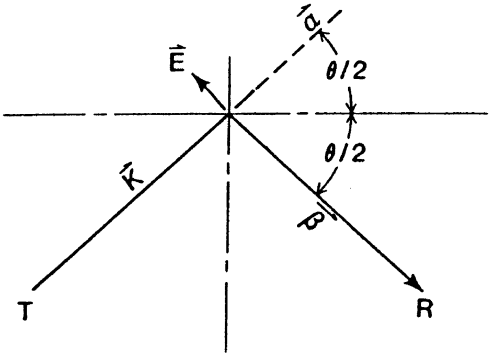

Figure 3.35. The geometry for scatter from ionospheric irregularities.

of the backscatter sounder, the mean fractional deviation in electron density of the scatterer, and the aspect angle between the radar LOS and the major axis of the irregularity. Figure 3.34 shows the approximate height–frequency domains of typical ionospheric sounding systems.

The first quantitative description of coherent scatter from ionospheric irregularities was published by Booker (1956) (an extension of the Booker–Gordon (1950) troposcatter theory), when he developed a theory that described backscatter from field-aligned irregularities in the auroral E region. The results are also applicable to backscatter from F-region irregularities. The geometry of scatter from an ionospheric irregularity is shown in Figure 3.35.

From the geometry in Figure 3.35, we can obtain one form of the Booker

Downloaded from Cambridge Books Online by IP 141.211.4.224 on Wed Mar 23 15:38:40 GMT 2016.
http://dx.doi.org/10.1017/CBO9780511535758.005
Cambridge Books Online © Cambridge University Press, 2016

ionospheric-irregularity scatter equation expressed in terms related to ionospheric parameters as

$$\sigma(\theta, \chi) = (\Delta N/N)^2 (2\pi L/\lambda_N)^2 \sin^2 \chi / \{\lambda_N [1 + (4\pi L/\lambda)^2 \sin^2(\theta/2)]\}, \qquad (3.126)$$

where $\sigma(\theta, \chi)$ is the backscatter cross-section of the irregularity, $(\Delta N/N)^2$ is the mean square fractional deviation in electron density, λ_N is the wavelength of plasma oscillation, and L is the scale size of the irregularity along **B**.

Relations for the backscatter cross-section in the cases of large and small irregularities are derived in Hunsucker (1991, p. 56). Walker *et al.* (1987) started with the Booker scattering equation and derived a more general expression for the backscattered power at the receiver (see also Hunsucker, 1991, pp. 56-58).

3.5.2 Forward scatter

Irregularities due to turbulence in the 75–90-km regions of the ionosphere permit one to design one-hop communication circuits at VHF (Bailey *et al.*, 1955; Norton and Wiesner, 1955). The *ionoscatter* mode typically uses frequencies from 30 to 60 MHz, over distances of 1000–2000 km with system losses of 140–210 dB and a usable bandwidth of ≈10 kHz. Because of the high system loss, very-high-power transmitters, large high-gain antennas and sensitive receiver front ends are required. Ionoscatter systems are also characterized by very high reliability and security, but use of this bandwidth probably involves the highest cost per system of all radio systems. In the late 1950s and early 1960s considerable use of the ionoscatter mode was made because of its 99.9% reliability and security, but, with the advent of satellite–Earth radio systems, use of the ionoscatter mode decreased drastically.

3.5.3 Incoherent scatter

The development of the incoherent-scatter radar technique has provided a very powerful method for investigating the ionosphere. Evans (1969 and 1972) summarised the essentials of incoherent-scatter theory and practice and rigorous derivations of the salient equations are given by Krall and Trivelpiece (1973).

The basic theory of scattering of electromagnetic waves from free electrons was developed by the discoverer of the electron, J. J. Thomson, who in 1906 showed that the energy scattered by a single electron is

$$W = (r_e \sin \psi)^2, \qquad (3.127)$$

where W is the energy scattered by a single electron into unit solid angle per unit of incident electromagnetic flux (1 W m^{-2}); r_e is the classical electron radius, $r_e = e^2/(\varepsilon_0 m_e c^2) = 2.82 \times 10^{-15}$ m; and ψ is the angle between the direction of the incident electric field and the direction of the observer.

Downloaded from Cambridge Books Online by IP 141.211.4.224 on Wed Mar 23 15:38:40 GMT 2016.
http://dx.doi.org/10.1017/CBO9780511535758.005
Cambridge Books Online © Cambridge University Press, 2016

The *radar cross-section* of an individual electron would then be

$$\sigma_e = 4\pi(r_e \sin\psi)^2 \approx 10^{-28}\sin^2\psi\,(\mathrm{m}^2)$$

and, for *backscatter* ($\psi = \pi/2$),

$$\sigma_e = 4\pi r_e^2. \tag{3.128}$$

Fejer (1960) showed that the radar cross-section per unit volume is simply

$$\sigma = N\sigma_e, \tag{3.129}$$

where N is the electron density, and Buneman (1962) showed that the incoherent scatter *effective radar cross-section* (σ_{eff}) can be written as

$$\sigma_{\mathrm{eff}} = 1/[(1+\alpha^2)(1+T_e/T_I+\alpha^2)] \tag{3.130}$$

for $T_e/T_I < 3.0$, and T_e is the electron temperature, T_I is the ion temperature, $\alpha = 4\pi D/\lambda$, where D is the Debye length, $D = 6.9(T_e/N_e)^{1/2}$, in centimeters, and λ is the free-space wavelength of the radar signal.

Since the electrons are in random thermal motion, they will scatter signals whose phases are varying with time and are not related to one another. At the radar-receiving antenna the signal *powers* will add so that, on the average, the cross-section per unit volume is that given by Equation (3.129), giving use to the name "incoherent scatter".

The interesting history of the development of incoherent-scatter theory and practice starting shortly after the end of WWII has been described by Davies (1990, pp. 106–111) and by Hunsucker (1991, pp. 58–64). Dougherty and Farley (1960) explained the discrepancy between the predicted and measured Doppler broadening of the echo spectrum in terms of the radar wavelength, electron and ion temperatures, and the Debye length,

$$D = 69(T_e/N_e)^{1/2}\ (\mathrm{m}), \tag{3.131}$$

Where T is in kelvins and N in m^{-3}.

Incoherent scattering occurs from fluctuations in electron density having a scale of D. The backscatter, then, is actually due to local fluctuations in electron density, instead of purely scatter from free electrons, and more correctly should be called something like quasi-incoherent scatter, but the term *incoherent scatter* has persisted. Some authors continue to refer to the incoherent-scatter phenomena as Thomson scatter for a variety of reasons; however, the term Thomson scatter is normally reserved for situations of scattering from free electrons without influence from ions.

In practice, this incoherent scatter is detected from the ionosphere principally

Downloaded from Cambridge Books Online by IP 141.211.4.224 on Wed Mar 23 15:38:40 GMT 2016.
http://dx.doi.org/10.1017/CBO9780511535758.005
Cambridge Books Online © Cambridge University Press, 2016

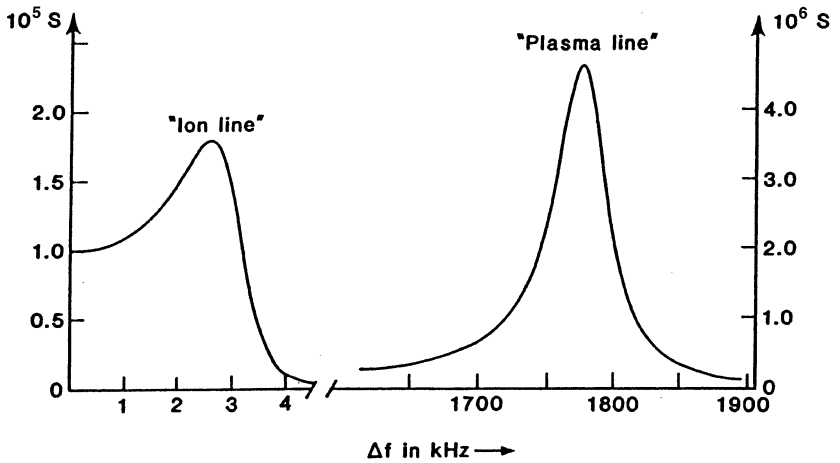

Figure 3.36. An idealized sketch of the ISR spectrum.

when $\lambda \gg D$, although experiments at Arecibo have detected incoherent scatter when $\lambda \approx D$ (Hagen and Behnke, 1976). The spatial scale of the irregularities λ_p is given by the Bragg formula,

$$\lambda_p = \lambda/[2\sin(\theta/2)] \tag{3.132}$$

with the geometry as shown in Figure 3.35.

The spectrum of an incoherent-scatter echo is very rich in information about the magnetoplasma which it is probing. A few of these plasma properties are easy to obtain, most requiring only straightforward data-analysis techniques, but some require complex processing using specific models of ionospheric regions.

Figure 3.36 is an idealized sketch of the spectrum of an incoherent-scatter echo from the ionosphere, showing the *ion line* on the left and the *plasma line* on the right. The ion line is centered on the operating frequency, f, and the energy back-scattered by irregularities of scale characterized by the Debye length that are in random motion, whereas the *plasma line* is centered on the plasma frequency f_N and is due to the thermal motions of electrons not under the influence of ions. The plasma line is a weak line, except when it is enhanced by "hot" photoelectrons; and when the line is enhanced, both the electron density and the characteristics of the photoelectron flux may be measured.

In the lower ionosphere the motions of the ions (which in turn control those of the electrons) are increasingly affected by collisions with the neutral air. The spectrum now becomes single-peaked, with width proportional to $T/(m_I \nu_I \lambda^2)$, where T is the temperature, m_i and ν_i are the mass and collision frequency of the ions, and λ is the wavelength of the radar. If $\lambda = 70$ cm and $T = 230$ K, the line is 1000 Hz wide at the height of 100 km, but, due to the increase of collision frequency, only a few hertz wide at 75 km.

Downloaded from Cambridge Books Online by IP 141.211.4.224 on Wed Mar 23 15:38:40 GMT 2016.
http://dx.doi.org/10.1017/CBO9780511535758.005
Cambridge Books Online © Cambridge University Press, 2016

In this, the *collision-dominated region,* the returned spectrum has the Lorentz form,

$$S(f) = A/[1 + f^2/(\Delta f)^2]. \tag{3.133}$$

(A is just a constant.) It is obviously much simpler than the F-region spectrum of Figure 3.44, and is fully described by its half-width:

$$\Delta f = 16\pi kT/(m_i \nu_i \lambda^2). \tag{3.134}$$

A Doppler shift is superimposed if the scattering volume is moving towards or away from the radar. The spectrum is somewhat broadened if negative ions are present. Equation (3.134) also assumes that the ion and electron temperatures are equal.

3.6 HF-propagation-prediction programs

In the last two decades, over a dozen HF-propagation programs have been developed for use on personal computers. Some representative examples are listed in Table 3.7. It should be emphasized that all these programs input median-value data and produce median values of MUF, LUF, signal strength, etc. as output and are basically intended for HF-circuit planning, not real-time prediction.

Most of the programs above take transmitter and receiver locations, time, month, year, and usually the number of sunspots as input, and provide MUF, LUF mode structure, antenna headings, great-circle distance and root-mean-square median-field-strength values for mid-latitude HF paths. The calculation of signal strength is especially difficult, because the exact mode structure on a particular path is not accurately known and all the path losses (in the D region, in the transmission line of the antenna, and from mismatch, ground reflection, etc.) are difficult to accurately characterize (see Sailors and Rose, 1991; and AGARDograph No. 326, 1990). Also, HF-propagation mode structure and losses at high latitudes are almost impossible to describe, so predictions of paths that include ionospheric reflections and points of D-region penetration in the auroral and polar ionosphere are almost useless (see Hunsucker, 1992; and discussions in Chapters 8 and 9 in this book).

There are several books covering the essentials of antennas, radio propagation at all frequencies, and related topics, such as those by Jordan and Balmain (1968), Sanders and Reed (1986), Rao (1977), Stutzman and Thiele (1981), Kraus (1988), Collin (1985), Hall and Barclay (1989), Freeman (1997), Balmain (1997), Hansen (1998), and Kildal (2000). There are also several recent books covering all aspects of *ionospheric* radio propagation and magnetoionic theory, such as those by Maslin (1987), Davies (1990), McNamara (1991), and Goodman (1992).

Downloaded from Cambridge Books Online by IP 141.211.4.224 on Wed Mar 23 15:38:40 GMT 2016.
http://dx.doi.org/10.1017/CBO9780511535758.005
Cambridge Books Online © Cambridge University Press, 2016

3.7 Summary

It is, of course, impossible to cover the entire topic of radio propagation in one chapter, but we have attempted to list the essential elements of pertinent terrestrial propagation modes and of antenna systems. It is fortunate that there are recent books available, which describe in considerable detail the particulars of these modes (Budden, 1985; Hall and Barclay, 1989; Davies, 1990; Goodman, 1992; Freeman, 1997). A very significant new development is the availability of PC or workstation-based software to analyze antennas, terrain and propagation prediction, as listed in the tables of this chapter. Another new development is the availability on the internet/www of URLs, which give near-real-time data for

Table 3.7. *Representative PC-based HF-propagation-prediction programs*

Name of program	Description	Source	References and remarks
AMBCOM	Includes some effects of the high-latitude ionosphere		Hatfield (1980)
ASAPS 2			IPS (1991)
FTZMUF2	foF2 and M3000 MUF–LUF (?)		Dambolt and Sussman (1988a, b)
FTZ4	Improved calculation of several parameters		
HFBC84			
HFMUFES4			Barghausen *et al.* (1969)
ICEPAC	Includes some effects of the high-latitude ionosphere		Stewart (1990), private communication W1FM (Lexington, MA)
IONOSOND			
MINIFTZ4	Field strength		Dambolt and Sussman (1988a, b)
MINIMUF	MUF, LUF		Rose (1982)
PROPHET			Rose (1982)
PROPMAN	MUF/LUF, signal strength,		Roesler (1990)
VOACAP	User-friendly shell for IONCAP		Lane (1993)

Note:
MUF, maximum usable frequency; LUF, lowest usable frequency.

Downloaded from Cambridge Books Online by IP 141.211.4.224 on Wed Mar 23 15:38:40 GMT 2016.
http://dx.doi.org/10.1017/CBO9780511535758.005
Cambridge Books Online © Cambridge University Press, 2016

radio-prediction purposes. One excellent example is the "space–weather", magnetospheric, and ionospheric data bases available from the U. S. NOAA Space Environment Center (http://www.sec.noaa.gov).

3.8 References and bibliography

Section 3.2

ARRL (1999) *The ARRL Antenna Book*. The American Radio Relay League, Newington, Connecticut.

ARRL (2000) *The ARRL Handbook*, 77th edition. The American Radio Relay League, Newington, Connecticut.

Balanis, C. A. (1997) *Antenna Theory, Analysis and Design*. Wiley, New York.

Hunsucker, R. D. (1991) *Radio Techniques for Probing The Terrestrial Ionosphere*. Springer-Verlag, Heidelberg.

Skolnik, M. F. (1980) *Introduction to Radar Systems*, 2nd edition. McGraw-Hill, New York.

Wolf, E. A. (1988) *Antenna Analysis*. Artech House, Norwood, MA.

Section 3.3

AGARDograph No. 326 (1990) *Radio Wave Propagation Modeling, Prediction and Assessment*, pp. 69–72. AGARD/NATO.

Andersen, J. B., Hvid, J. T., and Toftgard, J. (1993) Comparison between different path loss prediction models, COST 231-TD(93)-06, January, Barcelona.

Brent, R. I. and Ormsby, J. F. A. (1994) Electromagnetic propagation modeling in 3D environments using the Gaussian beam method. Joint Electronic Warfare Center Technical Report JDR 3-94.

CCIR Report 322-3c (1988) Characteristics and applications of atmospheric noise data. *XVth Plenary Assembly, Dubrovnik*. International Telecommunications Union, Geneva.

Chamberlain, K. and Luebbers. R. (1992) *GELTI Propagation Model: Theory of Operation and Users' Manual*. Available through the authors.

Collin, R. E. (1985) *Antennas and Radiowave Propagation*. McGraw-Hill Book Co., New York.

Eppink, D. and Kuebler, W. (1994) *TIREM/SEM Handbook*. DoD ECAC, Annapolis, Maryland.

Freeman, R. L. (1997) *Radio System Design for Telecommunications*. Wiley, New York.

Grosskopf, R. (1994) Propagation of urban propagation loss. *IEEE Trans. Antennas Propagation* **42**, 1–7.

Hansen, R. C. (1998) *Phased Array Antennas*. Wiley, New York.

Hey, H. S. (1983) *The Radio Universe*, 3rd Edition. Pergamon Press, Oxford.

Hunsucker, R. D. (1992) Auroral and polar cap ionospheric effects on radio propagation. *IEEE Trans. Antennas Propagation* **40**, 818–828.

Downloaded from Cambridge Books Online by IP 141.211.4.224 on Wed Mar 23 15:38:40 GMT 2016.
http://dx.doi.org/10.1017/CBO9780511535758.005
Cambridge Books Online © Cambridge University Press, 2016

Jordan, E. C. and Balmain, K. G. (1968) *Electromagnetic Waves and Radiating Systems*, 2nd Edition. Prentice-Hall, Inc., Englewood Cliffs, New Jersey.

Kraus, J. D. (1988) *Antennas*, 2nd Edition. Cygnus-Quasar Books, Powell, Ohio.

Marcus, S. (1994) Duct propagation over a wedge-shaped hill, *BLOS Proc.* Applied Research Laboratory, University of Texas, Austin, Texas.

Patterson, W. (1994) EM propagation program at NCCOSC, *BLOS Proc.* Applied Research Laboratory, University of Texas, Austin, Texas.

Rao, N. N. (1977) *Elements of Engineering Electromagnetics*. Prentice-Hall, Inc., Englewood Cliffs, New Jersey.

Ryan, F. J. (1991) *Analysis of Electromagnetic Propagation Over Variable Terrain Using the Parabolic Wave Equation*. Naval Ocean Systems Center, San Diego, California.

Sailors, D. B. (1993) *A Discrepancy in the CCIR Report #22-3 Radio Noise Model*. NCCOSC/NRaD, San Diego, California.

Sanders, K. F. and Reed, G. A. L. (1986) *Transmission and Propagation of Electromagnetic Waves*. Cambridge University Press, Cambridge.

Spaulding, A. D. and Washburn, J. S. (1985) *Atmospheric Radio Noise: Worldwide Levels and Other Characteristics*. ITS, Boulder, Colorado.

Vincent, W. R. and Munsch, G. F. (1996) *Power-line Noise Mitigation Handbook for Naval Receiving Sites*, 3rd Edition. COMMNAVSECGRU, Meade, Maryland.

Section 3.4

Appleton, E. V. (1930) Some notes on wireless methods of investigating the electrical structure of the upper atmosphere. *Proc. Phys. Soc.* **42**, 321.

Budden, K. G. (1961) *Radio Waves in the Ionosphere*. Cambridge University Press, Cambridge.

Budden, K. G. (1985) *The Propagation Of Radio Waves: The Theory of Radio Waves of Low Power in the Ionosphere and Magnetosphere*. Cambridge University Press, Cambridge.

Carpenter, D. L. (1988) Remote sensing of the magnetospheric plasma by means of whistler mode signals. *Rev. Geophys*. **26**, 535–549.

Crane. R. K. (1974) *Morphology of ionospheric scintillation*. Technical Note 1974–26, Lincoln Laboratory, MIT.

Davies, K. (1969) *Ionospheric Radio Waves*. Blaisdell Publishing Co., Waltham, Massachusetts.

Eckersley, T. L. (1925) Note on musical atmospheric disturbances. *Phil. Mag*. **49**: (5), 1250–1259.

Eckersley, T. L. (1928) Letter to the editor. *Nature* **122**,768–769.

Eckersley, T. L. (1929) An investigation of short waves. *J. Inst. Electr. Engineers* **67**, 992–1032.

Eckersley, T. L. (1931) 1929–1930 developments in the study of radio wave propagation. *Marconi Rev*. **5**: 1–8.

Eckersley, T. L. (1932) Studies in radio transmission. *J. Inst. Electr. Engineers*. **71**, 434–443.

Downloaded from Cambridge Books Online by IP 141.211.4.224 on Wed Mar 23 15:38:40 GMT 2016.
http://dx.doi.org/10.1017/CBO9780511535758.005
Cambridge Books Online © Cambridge University Press, 2016

Fraser-Smith, A. C. and Bannister, P. R. (1997) Reception of ELF signals at antipodal distances. *Radio Sci*. **32**.

Hargreaves, J. K. (1992) *The Solar–Terrestrial Environment*. Cambridge University Press, Cambridge.

Helliwell, R. A. (1965) *Whistlers and Related Ionospheric Phenomena*. Stanford University Press, Stanford, California.

Helliwell, R. A. (1988) VLF wave stimulation experiments in the magnetosphere for Siple Station, Antarctica. *Rev. Geophys*. **26**, 551–578.

Hunsucker, R. D. (1999) Electromagnetic Waves in the Ionosphere. In *Wiley Encyclopedia of Electrical and Electronics Engineering* (ed. J. Webster), pp. 494–506. Wiley, New York.

Kelso, J. M. (1964) *Radio Ray Propagation in the Ionosphere*. McGraw-Hill, New York.

Park, D. and Carpenter, D. (1978) Very low frequency radio waves in the magnetosphere. In *Upper Atmospheric Research in Antarctica* (ed. L. J. Lanzerotti and C. G. Parr). American Geophysical Union, Washington, DC.

Radio Science (1967). Special issue on analysis of ionograms for electron density profiles. *Radio Sci*., **2**, 1119–1282.

Ratcliffe, J. A. (1956) Some aspects of diffraction theory and their application to the ionosphere. Rep. Prog. Phys., **19**, 188.

Ratcliffe, J. A. (1959) *The Magneto-ionic Theory and its Application to the Ionosphere. A Monograph*. Cambridge University Press, Cambridge.

Smith, N. (1939) The relation of radio sky-wave transmission to ionosphere measurements. *Proc. IRE* **27**, 332–347.

Titheridge, J. E. (1985) *Ionogram Analysis with the Generalized Program POLAN*. World Data Center-A, NOAA, Boulder, Colorado.

Umeki, R., Liu, C. H. and Yeh, K. C. (1997a) Multifrequency studies of ionospheric scintillations. *Radio Science* **12**, 311.

Umeki, R., Liu, C. H. and Yeh, K. C. (1997b) Multifrequency spectra of ionospheric amplitude scintillations. *J. Geophys. Res* **82**, 2752.

URSI (1972) URSI handbook on ionogram interpretation and reduction, 2nd Ed., NOAA WDC-A, Rep. UAG-23, Boulder, Colorado.

Wait, J. R. (1970) *Electromagnetic Waves in Stratified Media*, 2nd Edition. Pergamon Press, New York.

Yeh, K.-C., Chao, H. Y. and Lin, K. H. (1999) A study of the generalized Faraday effect in several media. *Radio Sci*. **34**, 139.

Yeh, K.-C. and Liu, C.-H. (1982) Radio wave scintillation in the ionosphere. *Proc. IEEE* **70**, 324–360.

Section 3.5

Bailey, D. K., Bateman, R. and Kirby, R. C. (1955) Radio transmission at VHF by scattering and other processes in the lower in the lower ionosphere. *Proc. IRE* **43**, 1181.

Downloaded from Cambridge Books Online by IP 141.211.4.224 on Wed Mar 23 15:38:40 GMT 2016.
http://dx.doi.org/10.1017/CBO9780511535758.005
Cambridge Books Online © Cambridge University Press, 2016

Booker, H. G. (1956) A theory of scattering by nonisotropic irregularities with application to radar reflection from the aurora. *J. Atmos. Terr. Phys.* **8**, 204–221.

Booker, H. G. and Gordon, W. E. (1950) A theory of radio scattering in the troposphere. *Proc. Inst. Radio Engineers **38***, 401–402.

Buneman, O. (1962) Scattering of radiation by the fluctuations in a non-equilibrium plasma. *J. Geophys. Res*. **67**, 2050–2053.

Dougherty, J. P. and Farley, D. T. (1960) A theory of incoherent scatter of radio waves by a plasma. *Proc. R. Soc.* A **259**, 79.

Evans, J. V. (1969) Theory and practice of ionospheric study by Thomson scatter radar. *Proc. IEEE 57*, 496.

Evans, J. V. (1972) Ionospheric movements measured by incoherent scatter: A review. *J. Atmos. Terr. Phys*. **34**, 175.

Fejer, J. A. (1960) Scattering of radiowaves by an ionized gas in thermal equilibrium. *J. Geophys. Res. 65*, 2635.

Hagen, J. B. and Behnke, R. A. (1976) Detection of the electron component of the spectrum in incoherent scatter of radio waves by the ionosphere. *J. Geophys. Res*. **81,** 3441–3443.

Krall, N. A and Trivelpiece, A. W. (1973) *Principles of Plasma Physics*. McGraw-Hill, New York.

Nakajima, M. (1960) The m-distribution – A general formulation of intensity distribution of rapid fading. In *Statistical Methods in Radio Propagation* (ed. W. C. Hoffman). Oxford, Pergamon.

Norton, K. A. and Wiesner, J. B. (1955) The scatter propagation issue. *Proc. IRE* **43**, 1174.

Schlegel, K. (1984) *HF and VHF Coherent Radars for Investigation of the High-latitude Ionosphere*. Max Planck Institut für Aeronomie, Katlenburg-Lindau.

Walker, A. D. M, Greenwald, R. A., and Baker, K. D. (1987) Determination of the fluctuation level of ionospheric irregularities from radar backscatter measurements. *Rad. Sci*. **22**: 689–705.

Section 3.6

Barghausen, A. F., Finney, J. W., Proctor, L. L. and Schultz, L. D. (1969) Predicting Long-term Operational Parameters of High Frequency Skywave Telecommunications Systems. ESSA, Boulder, Colorado.

Damboldt, T. and Suessmann, P. (1988*a*) *FTZ High Frequency Sky-wave Field Strength Prediction Method for Use on Home Computers*. Forschungsinstitut der DBP beim FTZ.

Damboldt, T. and Suessmann P. (1988*b*) A Simple Method of Estimating foF2 and M3000 with the Aid of a Home Computer. Forschungsinstitut der DBP beim FTZ.

Davies, K. (1990) *Ionospheric Radio*. Peter Peregrinus, London.

Hatfield, V. E. (1980) HF communications predictions, 1978. (An economical up-to-date computer code, AMBCOM). In *Solar–Terrestrial Predictions Proc.* (ed. R. F. Donnelly), Vol. 4, D2 1–15. US Government Printing Office, Washington DC.

Downloaded from Cambridge Books Online by IP 141.211.4.224 on Wed Mar 23 15:38:40 GMT 2016.
http://dx.doi.org/10.1017/CBO9780511535758.005
Cambridge Books Online © Cambridge University Press, 2016

Jordan, E. C. and Balmain, K. G. (1968) *Electromagnetic Waves and Radiating Systems*, 2nd Edition, Prentice-Hall, Englewood Cliffs, New Jersey.

Lane, G. (1993) *Voice of America Coverage Analysis Program (VOACAP)*. US Information Agency, Bureau of Broadcasting, Washington DC.

Maslin, N. M. (1987) *HF Communications: A Systems Approach*. Plenum Press, New York.

McNamara, L. F. (1991) *The Ionosphere: Communications, Surveillance, and Direction Finding*. Krieger Publishing Co., Malabar, Florida.

Roesler, D. P. (1990) HF/VHF Propagation resource management using expert systems. In *The Effect of the Ionosphere on Radiowave Signals and Systems Performance (IES90)* (ed. J. M. Goodman), pp. 313–321. USGPO, available through NTIS, Springfield, Virginia.

Rose, R. (1982) An emerging propagation prediction technology. In *Effects of the Ionosphere on Radiowave Systems (IES81)* (ed. J. Goodman). US Government Printing Office, Washington, DC.

Sailors, D. B. and Rose, R. B. (1991) *HF Sky Wave Field Strength Predictions*. NCCOSC/NRaD, San Diego, California.

Section 3.7

Briggs, B. H. and Parkin, J. A. (1963) On the variation of radio star and satellite scintillation with zenith angle. *J. Atmos. Terrestr. Phys.* ***25***, 339.

Goodman, J. (1992) *HF Communications – Science and Technology*. Van Nostrand Reinhold, New York.

Hall, M. P. M. and Barclay, L. W. (eds.) (1989) *Radiowave Propagation*. Peter Peregrinus Press for the IEE, London.

Nakajima, M. (1960) The m-distribution – A general formulation of intensity distribution of rapid fading. In *Statistical Methods in Radio Propagation* (ed. W. C. Hoffman). Oxford, Pergamon.

General reading

Kildal, P.-S. (2000) *Foundations of Antennas – A Unified Approach*. Studentlitteratur, Lund.

Ramo, S., Whinnery, S., and van Duzer, T. (1965) *Fields and Waves in Communication Electronics*. Wiley, New York.

Downloaded from Cambridge Books Online by IP 141.211.4.224 on Wed Mar 23 15:38:40 GMT 2016.
http://dx.doi.org/10.1017/CBO9780511535758.005
Cambridge Books Online © Cambridge University Press, 2016